A First Principles Analysis of C−H Bond Formation in Ethylene Hydrogenation

Matthew Neurock*

Department of Chemical Engineering, University of Virginia, Charlottesville, Virginia 22903

Rutger A. van Santen

Schuit Institute of Catalysis, Department of Inorganic Chemistry, Technical University of Eindhoven, Eindhoven, The Netherlands

Received: November 17, 1999; In Final Form: July 24, 2000

The Horiuti−Polanyi mechanism for ethylene hydrogenation over Pd(111) is examined using first-principle density functional quantum chemical calculations. Cluster and periodic slab DFT-GGA calculations were carried out to determine the modes and energies of chemisorption for a sequence of proposed intermediates, along with overall reaction energies and activation barriers for each of the speculated elementary steps. The DFT-calculated binding energies for ethylene (π), ethylene (di-σ), ethyl, vinyl, ethylidyne, atomic oxygen, and atomic carbon on the Pd_{19} cluster (and the Pd(111) slab) were found to be −30 (−27), −60 (−62), −130 (−140), −237 (−254), −620 (−636), −375 (−400), and −610 (−635) kJ/mol. The slab results were found to be within 20 kJ/mol of the cluster results. Frequency calculations along with predicted chemisorption energies indicate that ethylene adsorbs in both π- and di-σ-configurations. At moderate temperatures, the binding energies for π- and di-σ-bound ethylene are comparable. At low surface coverages, the predicted intrinsic activation barriers are +72 kJ/mol for the hydrogenation of ethlyene to surface ethyl and +71 kJ/mol for ethyl to ethane. The corresponding overall reaction energies for these two steps are +3 and −5 (without lateral interactions) kJ/mol, respectively. At low surface coverages, the di-σ-intermediate appears to be the precursor to reaction. At low coverage the π-bound intermediate is first converted to the di-σ-species before it will react with hydrogen. The *apparent* activation barrier for ethylene hydrogenation to surface ethyl is 26 kJ/mol which is significantly lower than the intrinsic activation barrier. The apparent barrier is measured with respect to the gas-phase rather than the adsorbed ethylene state. Higher surface coverages alter the favored reaction state. At higher coverages, the activation barriers for ethylene hydrogenation to surface ethyl were calculated to be +82 and +36 kJ/mol for the di-σ- and π-bound intermediates, respectively. Higher surface coverages weaken both the metal−hydrogen and metal−carbon bonds. This promotes hydrogenation from the π-bound state. The calculated barrier of +36 kJ/mol (from the π-bound state) at higher surface coverages is consistent with experimentally reported ethylene hydrogenation barriers.

I. Introduction

The hydrogenation of ethylene has served as the classic model for understanding the hydrogenation of olefins and aromatics for nearly 75 years.[1a] Olefin hydrogenation is at the heart of petroleum hydrotreating and upgrading processes as well as saturated oil hydrogenation processes in the food industry. In addition to these bulk chemical processes, many current pharmaceutical and fine chemical syntheses target the selective the hydrogenation of specific olefin bonds. Suppported palladium and bimetallic palladium particles typically demonstrate both higher activities as well as selectivities over other metals. Examples include the hydrogenation of maleic anhydride/maleic acid to tetrahydrofuran which is effectively catalyzed over supported Pd/Re particles,[1b] and the selective hydrogenation of pyrazine-2-*tert*-butyl-carboxamide to the tetrahydro-pyrazine intermediate over Pd/C. This tetrahydro intermediate is subsequently hydrogenated using an asymmetric catalyst to form the chiral (*S*)-piperazine-2-butyl-carboxamide which is a critical intermediate in Merck's process to produce Crixivan.[1C] In addition to enhancing olefin hydrogenation activity, there are also a number of systems in which palladium is used to actually minimize olefin hydrogenation activity. Most notable is the production of polymer-grade ethylene from feedstocks which require the selective hydrogenation of acetylenic molecules without saturating ethylene. This chemistry is typically carried out over supported Pd/Ag particles so as to maintain high activity and minimize ethylene hydrogenation. In this work, we examine ethylene hydrogenation over Pd as a model for these chemistries.

Despite the tremendous number of studies on ethylene hydrogenation, there are still a number of features about the reaction mechanism that are still unknown. At least three general reaction paths have been proposed.[2] The first path involves a series of surface catalyzed hydrogen addition steps, and is known as the Horiuti−Polanyi mechanism.[3] In the second path, ethylene is first dehydrogenated before hydrogenation occurs. This was initially proposed by Farkas and Farkas.[4] The third path involves intermolecular hydrogen transfer from surface ethylidyne to coadsorbed ethylene intermediates.[5] Much of the experimental evidence that has been uncovered over the past decade strongly supports the Horiuti-Polanyi mechanism. The intermolecular hydrogen transfer mechanism has been ruled out by the detailed spectroscopic studies of Beebe and Yates.[6] Cremer and Somorjai[7−9] have also shown conclusively that the ethylidyne surface species are not directly involved in the mechanism and are only spectator species.

10.1021/jp994082t CCC: $19.00
Published on Web 10/28/2000

While the reaction is thought to follow the general features proposed by Horiuti−Polanyi, the specific details of how this occurs are yet to be determined. The controlling surface intermediates, the active surface sites, structure sensitivity, and the effect of coadsorbed surface species are all issues that are still actively debated.[1] Herein we report on a series of detailed first-principle quantum chemical results aimed at understanding the chemisorption and surface reactivity of ethylene on model Pd(111) clusters and surfaces. We analyze the overall reaction paths and energetics for hydrogenation via the Horiuti−Polanyi mechanism. In addition, we probe the effects of surface coverage on ethylene chemisorption and hydrogenation energetics.

II. Background

There have been numerous experimental investigations concerning the chemisorption and hydrogenation of ethylene. This literature can be readily categorized into studies on supported metals and studies on well-defined single-crystal metal surfaces. A number of excellent reviews on hydrocarbon chemisorption and hydrogenation already exist[1,10−12] which discuss some of the general factors that govern ethylene hydrogenation. We therefore only present some of the salient features of the chemistry here and encourage the interested reader to refer to the above reviews for more in-depth discussions.

Ethylene is thought to adsorb on single-crystal transition metal surfaces in one of three modes: π, di-σ, or physisorbed (π).[10,13a−c] Recent evidence indicates that a low-temperature physisorption state may also exist as a precusor state that is relevant for olefin hydrogenation.[13−15] In the π-bound chemisorption and physisorption modes, ethylene sits atop a single metal atom. In the di-σ-mode, ethylene binds parallel to one of the bridge metal−metal bonds forming two σ-metal−carbon bonds. The favored adsorption site is strongly dependent upon the electronic and the geometric structure of the exposed metal surface as well as the reaction conditions. Yagasaki and Masel have elegantly summarized the wealth of UHV studies for ethylene chemisorption on different metals at low temperature to assess periodic trends.[10,13] They find that there is a correlation between the interstitial electron density and the ethylene bond order. Ethylene bond orders were subsequently used to characterize whether ethylene chemisorbs in either the π- or di-σ-adsorption modes depending upon the specific degree of hybridization. The π-bound intermediate is mostly sp^2 hybridized (bond order 1.5−2.0) whereas the di-σ-intermediate is nearly sp^3 (bond order 1.0−1.5). In general, ethylene is thought to bind in the π-adsorption mode for metals to the far left and far right of the periodic table, whereas the di-σ-mode appears to be most prevalent mode for metals that are located at the center of the transition metal series. On Pt(111), the di-σ-mode[10,13] was found to be the most favored. On palladium, however, the story is less clear. High resolution electron energy loss experiments suggest that the spectra for ethylene on Pd(111) more closely matches the π-mode.[16−18] Stuve and Madix,[19,20] however, found that the distinction between π and di-σ ethylene is difficult to resolve over Pd(110), and suggested that both modes are present on the surface. They define the π/di-σ-parameter as a measure of the degree of π− to di-σ-character and site preference.

The favored adsorption site is also strongly dependent upon the *composition* as well as the *coverage* of different species present on the surface. At relatively moderate levels of oxygen, carbon or hydrogen, ethylene can move to other adsorption sites. This can be governed by through-space or through-surface lateral interactions. Stuve and Madix, for example, found that ethylene prefers to bind di-σ on the clean Pd(110) surface. In the presence of oxygen, however, the π mode is more favored.[19,20]

Most metal surfaces are likely to be covered with carbonaceous overlayers. Ethylene is known to readily dehydrogenate over most group VIII metals to form ethylidyne as well as other CH_x surface intermediates[1,11−13,21] all of which are very strongly bound to the surface. These species cover the surface and can subsequently go on to form surface bound polymers, graphite, or coke. Ethylidyne, which is one of the most abundant surface intermediates is primarily thought to be a spectator species and is not directly involved in the mechanism.[6,8,9,20,23] The secondary effects of having ethylidyne and other CH_x intermediates on the surface, however, have yet to be established. The formation of ethylidyne is thought to involve the interconversion of di-σ-bound surface ethylene. The di-σ-bound ethylene rather than the π-bound intermediate leads to the formation of dehydrogenation species. Ethylidyne can be formed by the intramolecular rearrangement to form ethylidene followed by C−H bond breaking.

The actual working surface of the catalyst is likely to have a distribution of π, di-σ ethylene species and ethylidyne surface intermediates.[1,8,9,22] The identification of the active precursor for ethylene hydrogenation has been based primarily upon speculation. On Pt(111), the di-σ-bound ethylene species was thought to be the active surface intermediate because it was present at higher surface concentrations than π-bound ethylene. Cremer and Somorjai,[7−9,22]however, have recently been able to provide the first substantial proof that the active species in ethylene hydrogenation over Pt(111) is actually the more weakly bound π-intermediate. They followed the dynamic changes in the infrared spectra for ethylene hydrogenation at higher pressures using sum frequency generation. They were able to selectively block the di-σ-adsorption sites without critically affecting the amount of π-bound ethylene species. The measured rate was found to be invariant with changes in the surface di-σ ethylene coverage. The π-bound intermediate, which occupies only 4% of the surface, is therefore thought to be responsible for the measured activity. Similar ideas were also reported by Zaera[24,25] and Merrill and Madix[26] for Pt(111) and Fe(100) surfaces. Zaera[24,25] used reflective absorption infrared spectroscopy (RAIRS) to show that at higher coverages the di-σ ethylene on Pt(111) is transformed into the more weakly adsorbed π-bound ethylene over Pt. The π-intermediate is suggested to react more readily with hydrogen. Merrill and Madix[26] showed that preadsorbed hydrogen forced ethylene to sit in the π-bound mode and thus increased its reactivity on Fe(100). In very recent kinetic Monte Carlo simulation studies, we found that the repulsive interactions between ethylene molecules on the surface can begin to stabilize π-bound ethylene species and lower their intrinsic activation barrier.[27]

The hydrogenation of ethylene follows different reaction orders depending upon specific processing conditions. In general, the reaction has been found to be 0 to −1 order in ethylene and 0.5−1.0 order in hydrogen.[1,6] The kinetics on well-defined surfaces and supported metal catalysts were found to be quite similar. The reaction is therefore thought to be structure insensitive.[1]

In very recent studies of ethylene hydrogenation on Pt(111), Janssens et al.[28] were able able to back out a more complete sequence of the selective and unselective steps in the hydrogenation of ethylene by using laser-induced thermal desorption reflection−absorption infrared spectroscopy and deuterium labeling to establish the H/D exchange. Ethylene adsorbs in both

π- and di-σ-adsorption states.[28−31] The π-bound mode exists at very low temperatures and at higher temperatures in the presence of other coadsorbates.[28,31] The π-bound intermediate is thought to lead to hydrogenated products whereas the di-σ-bound species is thought to lead to the formation of ethylidyne. Adsorbed ethylene can ether hydrogenate to form ethyl and subsequently ethane or decompose to form vinyl or ethylidene.[31−37] Ethylidene readily reacts to form ethylidyne. This sequence of steps is thought to occur quite readily. H/D exchange takes place at temperatures below which decomposition can take place. The exchange is therefore thought to be between the forward hydrogenation path which forms the labeled surface ethyl intermediate and the reverse C−H bond activation to convert ethyl back the ethylene. The reactions of ethylene to form ethylidene and ethylidene to ethylidyne occur at higher temperatures and have activation barriers that are on the order of 15−18 kcal/mol. The barriers are about 3−7 kcal/mol higher than that for the hydrogenation of ethylene to ethyl. The surface chemistry was found to be strongly dependent upon the surface coverage and reaction conditions. The results depend not only upon the coverage but on the specific surface structures that form. Recent STM studies indicate that the decomposition of ethylene to form ethylidyne requires a specific surface ensemble.[38]

The application of theory to ethylene hydrogenation has, for the most part, been qualitative. The studies by Hoffmann,[39−40] Sautet,[41] Siegbahn,[42−44] and Anderson[23] have been invaluable in understanding many of the relevant features such as the nature of bonding at different surface sites and the changes in adsorption energy with changes in the metal electronic and surface structure. Hoffmann and Silvestre[39] showed that ethylene was most stable in the di-σ-bound configuration on Pt(111) and demonstrated the mechanism to be the classic donation/back-donation model of Dewar−Chatt. Sautet and Paul,[41] used semiempirical Extended Hückel theory to show that the di-σ-bound ethylene species was favored on both Pd(111) and Pt(111). They suggested that this coordination mode is favored when there is a decrease in the repulsive interactions between the filled frontier orbitals of ethylene and occupied states in the valence band. This occurs when the coordination number about the metal center is reduced, such as at corner or edge sites. More recently Sautet,[45] Neurock,[46] King,[47] and van Santen[48,49] have used first-principle DFT cluster and slab calculations to show that that ethylene binds to Pd(111), Pt(111) and Ni(111) surfaces most favorably in the di-σ-adsorption mode. Their predicted adsorption energies are in very good agreement with known experimental values.

Siegbahn,[44] Hoffmann,[40] and Anderson [23] provided some of the early pioneering efforts toward understanding the mechanism for ethylene hydrogenation over homogeneous complexes and well-defined surfaces. Thorn and Hoffmann[40] were the first to present the "slip" mechanism whereby ethylene and hydrogen are bound in a square-planar configuration to the $Pt(PH_3)_2$ complex. The most reactive complex is one in which ethylene and hydrogen lie in the same plane cis to one another. As ethylene and hydrogen are brought together, the ethylene "slips" from the π-bond coordination to a state which has only a single sigma bond with one of the carbon atoms. The second CH_2 group moves away from the metal atom center in order to form a bond with the approaching hydrogen. The four-center transition state that is formed is sketched in Chart 1. The activation barrier for this step is critically controlled by the energy cost associated with distorting the angle α between the two adjacent ligands and the Pt center. Siegbahn et al.[44] performed higher level ab initio CI calculations on the homogeneous H−M−ethylene complex, where M refers to the central metal atom, to examine the general trends as one moves across the periodic table. They found that the transition state was similar to that proposed by Thorn and Hoffmann involving the "slip" of π-bound ethylene. The C−H bond is formed at the expense of breaking the M−H and M−C bonds. The main difference between metals is embodied in the repulsion between the electrons in occupied orbitals of ethylene and the nonbonding electrons of the metal. For single metal atom complexes, transition metals that lie to the left in the periodic table tend to have lower barriers because they can take advantage of the empty d-states to reduce this repulsion. The barrier height over Pd computed from the adsorbed H−Pd−ethylene complex was found to be +103 kJ/mol. This is significantly higher than that for T_c (+56 kJ/mol) and Mo (+75 kJ/mol) which are located further to the left in the period table. This was attributed to the greater repulsion with the increased number of accessible d-electrons. While there was no clear trend between the predicted barriers and the M−ethylene or M−H bond strengths, there was a dramatic lowering of the activation barrier as the number of hydride ligands were increased.

CHART 1

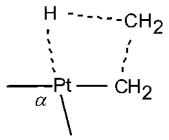

Anderson et al.[23] examined the effect of a (2×2) overlayer coverage of ethylidyne on Pt(111) in the hydrogenation of ethylene. They found that even though ethylidyne is strongly adsorbed to the surface, it is still highly mobile on Pt and can readily diffuse to new sites to enable ethylene to coadsorb. They concluded that ethylidyne does not dramatically affect the energetics for ethylene hydrogenation. They computed the activation energy for the reverse step, β-C−H bond activation of adsorbed ethyl to ethylene and hydrogen, to be +90 kJ/mol. This is about two times higher than that what was reported from UHV single-crystal studies (+47 kJ/mol). They also determined that the overall energy for the reaction for the dissociative adsorption of ethylene to form adsorbed ethylidyne and hydrogen is exothermic by 200 kJ/mol. This suggests that the reaction is quite favorable.

Herein we present the results of first-principle quantum chemical calculations toward understanding the chemisorption and surface reactivity of ethylene on model Pd(111) surfaces. We examine the energetics for a detailed sequence of the overall reaction paths and probe the atomic details of the mechanism. In addition, we explicitly probe the effects of coadsorbed carbon and oxygen on the local electronic structure and computed energies in order to understand the catalytic properties of the surface at higher coverage.

III. Computational Methods

First-principle density functional quantum calculations were carried out to examine the structure and energies for the reactants, products, and transition state complexes required for the hydrogenation of ethylene over Pd(111). We performed a series of calculations on cluster and periodic slab models of the Pd(111) surface in order to compute adsorption, lateral interaction, and activation energies. The gas-phase structures as well as the adsorbate/surface structures were optimized to determine the favored modes of adsorption along with the

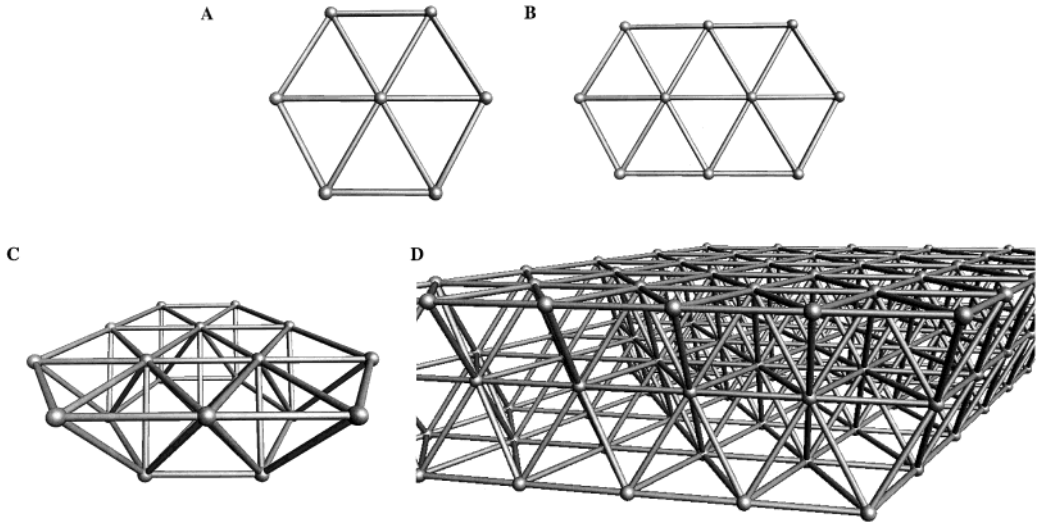

Figure 1. The cluster and slab models used to represent the Pd(111) surface: (A) Pd_7 was used to map out initial reaction paths and (B) Pd_{10} was used to compute frequencies, whereas (C) Pd_{19} and (D) the periodic three-layer Pd slab were used to compute the final energies.

corresponding energies of adsorption. Vibrational frequencies for both and di-σ-bound ethylene on model Pd(111) clusters were calculated to compare against known UHV electron energy loss spectra. Lateral interactions between adsorbates, which are known to significantly alter measured energies, were also computed. All of these energies were subsequently used to construct an overall potential energy diagram for the Horiuti−Polanyi mechanism. Detailed reaction coordinate analyses were subsequently performed to isolate the transition states and compute activation barriers for individual steps in the mechanism.

A. Cluster Calculations. The three cluster models (Pd_7, Pd_{10} and Pd_{19}) presented in Figure 1 were used to compute the results reported herein. The Pd_7 and the Pd_{10} clusters were used to gain preliminary insights into the governing features of the reaction coordinate and to calculate vibrational frequencies. Transition state searches and vibrational frequency calculations both required the calculation of numerical second derivatives of the energy with respect to the changes in the nuclear coordinates. This is computationally very expensive. The Pd_7 and Pd_{10} clusters provide a bare minimum in terms of cluster size for examining the structure, energy, and frequencies for reactants, products, and intermediates. The computed adsorption and binding energies on the Pd_7 and Pd_{10} clusters are likely to be overpredicted due to the presence of unsaturated metal coordination sites. Frequencies, however, were less sensitive to cluster size effects.[50−52] The larger Pd_{19} cluster and the infinite Pd slab provide much more realistic pictures of the electronic structure, and were therefore used to compute all final energies reported herein. Structural optimizations on Pd_{19} cluster, however, required nearly 12 CPU hours on a Cray C90. The calculation of frequencies are based on numerical second derivatives calculations and would have required weeks or months of valuable CPU resources. All frequency calculations were therefore performed on the moderate sized Pd_{10} cluster which captures the essential features of the surface and provides a reasonable estimation of the vibrational spectra.

All cluster calculations described herein were carried out using spin-polarized DFT calculations with nonlocal gradient corrections for the correlation and exchange energies. Density functional theoretical methods solve a series of single-particle Kohn−Sham equations. This is done iteratively to converge on the electron density and the overall electronic energy of the system in a self-consistent manner.[51,53−55] Analytical derivatives are computed after each SCF cycle and used to establish the relative changes in the nuclear coordinates for subsequent geometry optimization steps. All calculations used the Vosko−Wilk−Nusair (VWN) exchange−correlation potential[56] with Becke[57,58] and Perdew[59] nonlocal gradient corrections for the exchange and correlation terms, respectively. Nonlocal corrections were computed at every iteration within each self-consistent field cycle. The density and energy of each SCF cycle were converged to within 1×10^{-3} and 1×10^{-5} au respectively. Geometries for all structures were optimized to within 1×10^{-3} au.

DFT-optimized double-ζ Gaussian type orbital basis sets which include spin polarization were employed for all atoms.[53,61,62] These bases tend to perform one level higher in accuracy than their corresponding conventional ab initio molecular orbital basis.[53,61,62] Palladium is described by a pseudopotential[63] which explicitly includes scalar relativistic corrections. Nakao et al.[64] demonstrated that the correct structure, energy and spin state for even the palladium dimer required treating relativistic effects. Subsequent calculations on palladium clusters (Pd_1−Pd_{19})[46,65,66] demonstrated that relativistic corrections, along with spin state and geometry optimizations, were necessary for reliable predictions of structure and energetics in these systems. The results for a series of bare Pd_x clusters ($x = 1-19$) as well as clusters with atomic oxygen and ethylene bound to them are shown in Table A1 of the appendix. Although the spin is optimized within the self-consistent field, it is still necessary to specify the system's multiplicity in order to establish the lowest energy states. We performed calculation for different multiplicities for different size and shape Pd clusters to establish the lowest energy conformations and spin states. Our results for these systems indicate that the triplet spin states are consistently lower than the singlet spin states by 10−40 kJ/mol. In addition we compared the triplet spin state with the quintet state for some of the smaller Pd clusters as well as the Pd_{18} cluster and found that the triplet state was at least 30 kJ/mol more stable in energy. We also computed the optimal spin states for ethylene/Pd and O/Pd systems and once again the triplet was found to be the lowest energy state. On the basis of these calculations, we assumed that the optimal spin states for all other intermediates were triplet states. While we have not performed this complete spin-state analysis on each system, we believe that there is very little change in the calculated energies differences. If we are consistent in how we calculate differences

for adsorption, reaction, or activation energies, then these perturbations (10−30 kJ/mol) for the most part cancel out.

In all cluster calculations, except for those specified, the Pd cluster was held *fixed* at the metal positions of the ideal surface. The adsorbates were allowed to completely optimize. In early studies, we reported that surface relaxation phenomena, while important, contributed to less than 5 kcal/mol to the overall adsorption energy.[46,52,66,68]

B. Periodic Slab Calculations. To examine higher coverage situations and the effects of surface relaxation, we performed periodic DFT calculations. The periodic Pd(111) surface was described by constructing a supercell which is reproduced periodically along the lattice vectors that lie in the surface plane to describe either a $(\sqrt{3} \times \sqrt{3})$ $R30°$ or a (2×2) structure. The surface (or slab) structure consists of three Pd layers with the adsorbates bound to the top surface layer as shown in Figure 1D. A vacuum layer of 10 Å was placed above the adsorbate surface to avoid any electronic interactions between the slabs. The entire slab including the vacuum layer was then repeated along the lattice vector perpendicular to the surface. In previous calculations we examined the effect of the number of metal layers on the binding energies for hydrogen on Pd(111) and found that the energy changes were less than 1 kcal/mol as the slab thickness was increased to three layers and beyond.[69] In addition, the structural changes which occur in going beyond three layers were found to be negligible. Three layers of Pd therefore appear to provide a computationally efficient and tractable model of the surface.

All periodic calculations were performed using the plane-wave DFT code developed by Hammer, Nørskov, and Hansen.[70] The Kohn−Sham (KS) equations were solved using a plane wave basis set having a maximum kinetic energy of 40 Rydberg. Eighteen special *k*-points (Bloch vectors) were used in the description of the first Brillouin zone. The special *k*-points were chosen based on symmetry by the method developed by Chadi−Cohen.[71] Electron occupations were distributed according to a Fermi distribution corresponding to a thermal energy of $k_BT = 0.1$ eV. All final energies however were extrapolated back to $k_BT = 0.0$ eV. The KS equations were solved by using conjugate gradient minimization of the total energy followed by a subsequent damped density convergence scheme. All calculations were performed using nonlocal exchange and correlation potentials self-consistently in the form of the Perdew−Wang 91 generalized gradient corrections.[59] Scalar relativistic corrections were described through the use of norm-conserving pseudopotentials.[60,70] As discussed above, the surface is modeled using three palladium layers. The first two palladium layers were allowed to relax in an effort to understand the effects of surface relaxation. The bottom layer was held fixed at bulk structure of Pd(111). Adsorbates were then spaced in either a $(\sqrt{3} \times \sqrt{3})$ $R30°$ or a (2×2) surface structure. The $(\sqrt{3} \times \sqrt{3})$ $R30°$ structure was found to lead to repulsive interactions between neighboring ethyl intermediates. The (2×2) structure was therefore used to help eliminate any through-space repulsive interactions. The geometries of the first two layers of the surface along with the adsorbates structure were completely optimized.

C. Energy Calculations. Chemisorption energies were computed by subtracting the energies of the optimized gas-phase adsorbate and metal surface (cluster) from the energy of the optimized adsorbate−metal complex as shown in eq 1.

$$\Delta E_{\mathrm{Ads}} = E_{\mathrm{Adsorbate/Metal}} - E_{\mathrm{Adsorbate}} - E_{\mathrm{Metal}} \qquad (1)$$

Overall reaction energies were predicted in a similar manner as shown in eq 2 where the energies of the products are subtracted from the energies of the reactants.

$$\Delta E_{\mathrm{rxn}} = \sum E_{\mathrm{products}} - \sum E_{\mathrm{reactants}} \qquad (2)$$

The conventions used herein report adsorption energies and exothermic energies of reaction as negative values in that they release heat and follow the constructs of eqs 1 and 2.

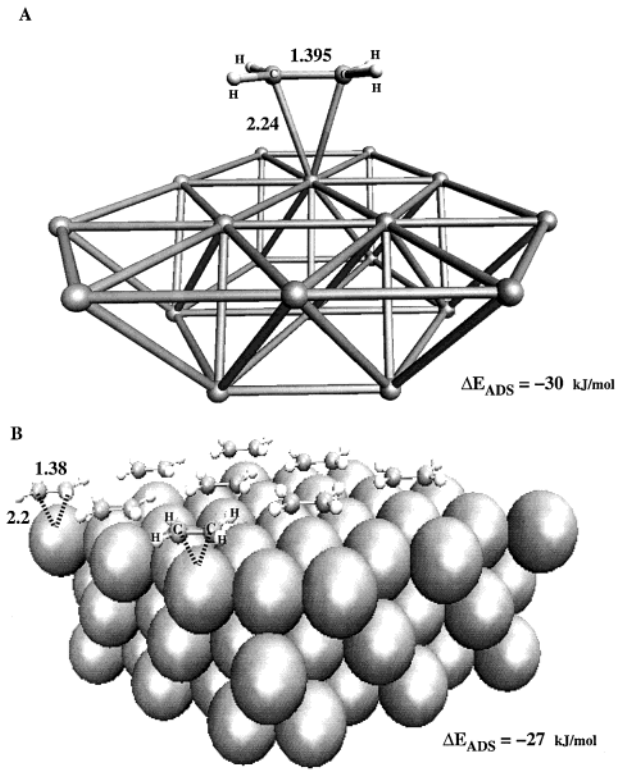

Figure 2. The chemisorption of ethylene in the π-bound mode on (A) the Pd_{19} cluster and (B) the three-layer Pd slab models of the Pd(111) surface.

IV. Results and Discussion

The reactive surface intermediates and hence the reaction energetics were found to change with different surface coverages. This has an important impact on the stability and activity of different reactive surface intermediates. The results are therefore broken down into discussions of the ideal low coverage situation and the more complicated high coverage reaction analyses.

A. Low Coverage Surface Intermediates and Reaction Paths. *1. Ethylene Chemisorption.* In an early paper we discussed the structures and energies of ethylene adsorption on model Pd_{19} clusters.[46] We highlight the important features here and add a more detailed analysis since it is relevant in understanding the hydrogenation reaction pathways. The optimized structures and energies for ethylene chemisorbed on the clean Pd(111) surface in both π- and di-σ-adsorption sites are shown in Figures 2 and 3, respectively. The chemisorption energies for all calculated surface intermediates are given in Table 1. In the π-adsorption mode, ethylene interacts with the surface through a weak van der Waals interaction. The classic Dewar−Chatt−Duncan model of orbital interactions can be used to describe the fundamental features of ethylene adsorption.[39] There is charge transfer from the σ orbitals of ethylene into the empty metal d-states at the surface, and in addition, the back-donation of electron density from the occupied metal d-band

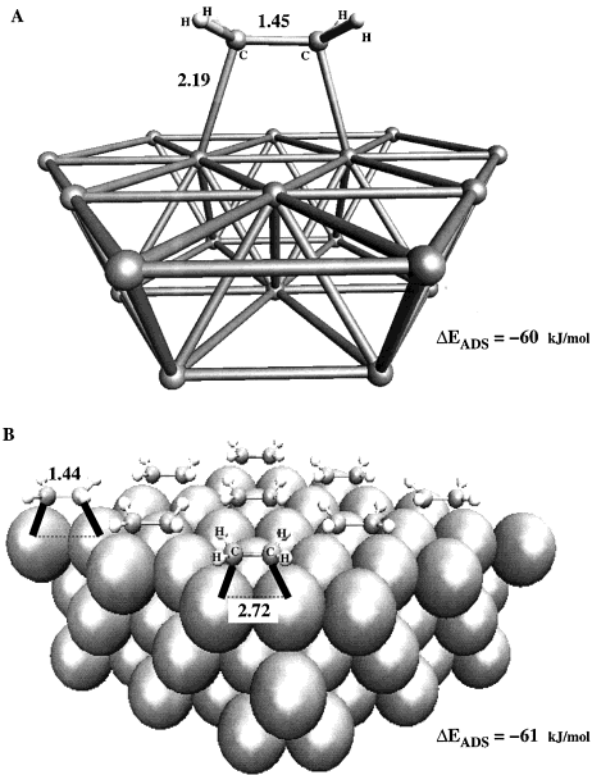

Figure 3. The chemisorption of ethylene in the di-σ-bound mode on (A) the Pd_{19} cluster and (B) the three-layer Pd slab models of the Pd-(111) surface.

TABLE 1: DFT-Calculated Adsorption Energies for C_2H_x and Atomic Surface Intermediates on the Pd19 Cluster and the Pd(111) 2 × 2 Three-Layer Slabs

species	ΔE_{ADS} Pd_{19} (kJ/mol)	ΔE_{ADS} Pd (111) 2 × 2 (kJ/mol)	experiment (kJ/mol)
ethylene			
(di-σ)	−60	−62	−59[18]
(π)	−30	−27	
vinyl			
$\eta^2(\mu^1,\mu^2)$	−237	−254	
ethyl			
atop	−130	−140	
bridge	−75		
ethylidyne			
3-fold fcc	−620	−636 ($CH_3C^{\cdot}$ quartet) −511 ($CH_3C^{\cdot}$ doublet)	
3-fold hcp	−603		
bridge	−587		
atomic hydrogen	−271	−266	−262[92]
atomic oxygen	−375	−400	
atomic carbon	−610	−635	

into the antibonding π*-orbital. This leads to an elongation of the carbon−carbon bond by 0.095 Å (1.395 Å) from gas-phase ethylene at 1.30 Å and a decrease in the bond order from 2.0 to 1.7 (see Figure 4). The carbon atoms remain nearly sp^2 hybridized. The predicted binding energy for the π-bound adsorption of ethylene on the Pd_{19} cluster was −30 kJ/mol (Figure 2A). The predicted binding energy on the Pd(111) slab was nearly the same at −27 kJ/mol (Figure 2B). Because of the relatively weak interaction between ethylene and the surface, the degree of surface relaxation was found to be negligible. The dominant orbital interactions involve the donation and back-donation of charge between the metal d-states and the highest occupied and lowest unoccupied orbitals of ethylene. A plot of the eigenvalues reveals that both π- the and π*-orbitals are located −5.09 and −3.66 eV below the highest occupied orbital

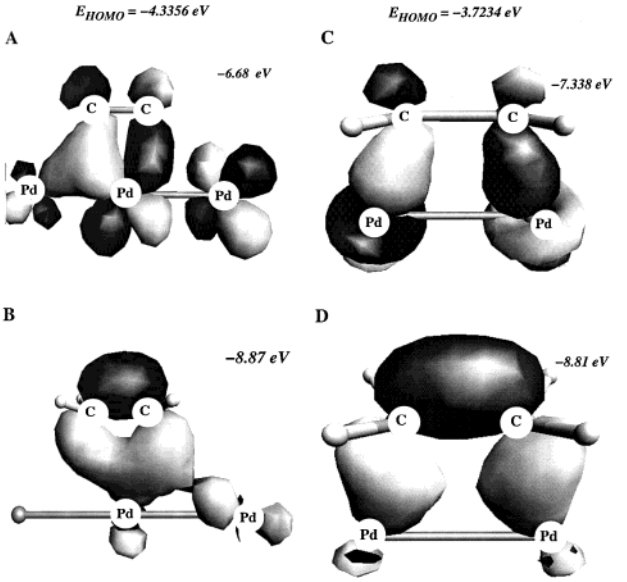

Figure 4. The frontier orbital interactions which control ethylene chemisorption on Pd. The highest occupied π-orbital of ethylene donates electron density into empty d_{z^2} surface states for both (A) the π-bound adsorption state and (C) the di-σ-adsorption state. The filled metal d_{xz} and d_{z^2} states back-donate electron density into the lowest unoccupied orbital π* orbital of ethylene into (B) the adsorption state and (D) the di-σ-adsorption state.

respectively due to enhanced orbital overlap with metal d_{z2}- and d_{xz}-metal surface states. The primary interactions between the π*- and π-orbitals of ethylene π-bound to palladium are depicted in Figure 4A,B.

The frequencies along with the relative intensities for each of the bands for π and di-σ-bound ethylene on Pd_{10} are reported in Tables 2 and 3. Metal−carbon bond stretching modes appear at 239, 369, and 569 cm^{-1} which are in good agreement with the EELS values of 256, 341, and 533 cm^{-1} reported by Gates and Kesmodel.[16] CH_2 bending modes begin to appear at 568, 751, 858, and 871 cm^{-1}. In addition to bending contributions, they also contain components of metal−carbon stretching. The calculated modes between 1000 and 1200 cm^{-1} involve coupled C═C stretching and CH_2 bending motions. Similar modes in the EELS data appear at 1078, 1145, and 1229 cm^{-1} but have been attributed only to the H−C−H bending modes. Neglecting the C═C stretch contributions in these modes tends to overestimate the relative amount of the π-bound surface. Our results are consistent with the analysis presented by Stuve and Madix[19,20] who indicated that the bands near 1200 cm^{-1} on Pd-(100) are likely due to coupled CH_2 bending and C═C stretching modes. The band present at 1500 cm^{-1} was also comprised of coupled C═C stretch and CH_2 bending modes. The location of this band (1500 cm^{-1}) corresponds well with the peak in the HREELS spectra at 1502 cm^{-1}. The calculated bands present at 3015−3050, and 3100 cm^{-1} correspond to the symmetric and antisymmetric C−H stretching modes. These modes appear experimentally over a very broad range between 2780 and 3000 cm^{-1}. Gates and Kesmodel[16] attribute the broad width of this band to weak metal−hydrogen interactions. Our calculations, however, indicate that there are essentially no interactions between the metal and the ethylene hydrogen atoms. The ethylene molecule in the π-mode remains very close to its gas-phase structure. The broad range of the distribution that appears in the experimental HREELS results instead may be due to the presence of both π- as well as di-σ-adsorption intermediates. The di-σ species have C−H stretching modes that appear at characteristically lower frequencies than that for the π-bound

TABLE 2: Comparison of Expermentally Reported Vibrational Frequencies from HREELS[14,15] and Those Calculated Here Using DFT Calculation and a Pd_{10} Cluster for the π-Adsorption Mode of Ethylene

experimental		DFT-calculated (Pd_{10} Cluster)		
mode	freq	freq (cm^{-1})	rel intens	key features
ν_{MC}	256	38.5	19.0	
ν_{MC}	341	49.5	0.9	
ν_{MC}	533	54.6	17.3	
		65.7	22.9	
HCH	691	72.9	9.5	
bending	911	76.5	18.1	
	1078	82.8	1.7	
	1145	84.7	12.6	
	1229	95.9	0.6	
		101.1	8.1	
δ_{CH2}	1418	108.5	4.5	
ν_{CC}	1502	117.2	28.5	
ν_{CH}	2780	122.7	106.8	
ν_{CH}	2996	137.3	0.9	
		146.9	130.5	
		162.5	69.5	
		203.9	269.7	
		239.7	1066.4	M−C stretch with H−C-M bending
		368.9	3940.0	M−C asymmetric stretch
		463.2	37472.7	M−C symmetric stretch
		568.9	2009.2	M−C stretch with CH_2 scissor
		751.5	423539.2	CH_2 wag with M−C stretch
		858.5	1585.2	CH_2 wag with M−C stretch
		872.0	16016.5	CH_2 deformation
		1010.6	329541.8	CH_2 deformation
		1178.5	116415.5	CH_2 deformation with C═C stretch
		1225.0	113757.4	C═C with HCH bend
		1496.3	109620.3	C═C stretch with symmetric HCH bend
		1500.5	39618.2	C═C with asymmetric HCH bend
		3015.9	12380.0	C−H symmetric stretch
		3049.4	99727.0	C−H stretch
		3098.5	111362.4	C−H symmetric stretch

TABLE 3: Comparison of Expermentally Reported Vibrational Frequencies from HREELS[14,15] and Those Calculated Here Using DFT Calculation and a Pd_{10} Cluster for the Di-σ-Adsorption Mode of Ethylene

experimental		DFT-calculated (Pd_{10} Cluster)		
mode	freq	freq (cm^{-1})	rel intens	key features
ν_{MC}	256	42.9	4.8	
ν_{MC}	341	49.8	2.5	
ν_{MC}	533	61.0	0.9	
		63.2	0.5	
HCH	691	71.5	0.3	
bending	911	75.3	6.1	
	1078	90.5	2.9	
	1145	94.7	1.3	
	1229	100.7	4.2	
		110.7	8.0	
δ_{CH2}	1418	116.6	2.3	
ν_{CC}	1502	120.6	5.0	
ν_{CH}	2780	131.4	17.2	
ν_{CH}	2996	139.3	7.4	
		141.6	12.9	
		169.5	14.7	
		184.3	48.2	
		233.1	163.2	M−C stretch with H−C-M bending
		260.6	4.6	M−C asymmetric stretch
		481.1	7.6	M−C symmetric stretch
		586.6	203.1	CH2 wag
		740.5	79.5	CH_2 wag
		844.2	34.5	CH_2 bending
		916.1	13.5	CH_2 bending
		967.7	971.9	CH_2 bending with C═C stretch
		1131.5	407.8	C═C stretch with CH_2 bending
		1217.7	73.7	CH_2 bending with C═C stretch
		1379.0	812.2	CH_2 bending with C═C stretch
		1443.5	742.7	C═C with asymmetric CH_2 bend
		2909.2	168.6	C−H stretch
		2961.7	55.2	C−H stretch
		3020.8	146.1	C−H stretch
		3063.0	1810.3	C−H stretch

intermediates. This is because the carbon atoms are sp^3 hybridized in the di-σ-mode and the C−H bond has less s-character. Gates and Kesmodel[16] had also indicated that the broad distribution could be due to the presence of other adsorption modes.

The optimized di-σ ethylene/Pd adsorption complex is depicted in Figure 3A and B. The di-σ-species appears to be more strongly bound to the surface than the π-bound intermediate. The energy of adsorption of ethylene in the di-σ-mode is −60 kJ/mol (−62 on Pd(111) slab), which is 30 kJ/mol stronger than that of π-bound ethylene. There is a substantial degree of back-donation from the surface as the C═C bond elongates by 0.12 Å to 1.45 Å thus becoming more like a C−C single bond. The hybridization about each of the carbon atoms reflect this change in character as they become much more sp^3-like. This can also be seen by the change in the H−C−C−H torsion angle from 180° for ethylene in the gas phase to 162° for π-bound ethylene and to 143° for di-σ-bound ethylene. The frontier orbital interactions for the di-σ-adsorption mode are plotted in Figure 4 C and D show the distinct interaction between the filled orbital of ethylene with a hybridized d_{z^2}-orbital of the metal (Figure 4D) as well as the back-donation of electron density from a hybridized d_{z^2}-state into the π^*-orbital (Figure 4C). The π^* and states π lie −3.62 and −5.09 eV below the energy level of the highest occupied orbital.

The vibrational frequencies for the di-σ-adsorption mode are shown in Table 3. The metal−carbon, CH_2 bending/C═C stretching modes, and the C−H stretch modes appear at 256, 341, 587, 968−1131, and 3020−3063 cm^{-1}, respectively. The results are very similar to those found for the π-bound mode as well as those reported from experiment. The primary differences between the π- and di-σ-adsorption modes reside in the distinction between the C═C stretching and CH_2 angle bending modes. Calculation results show that these modes are actually coupled. The strong features at 1225 and 1501 cm^{-1} that are characteristic of the CH_2 and C═C modes for the π-bound mode are not present in the spectra for the di-σ-bound ethylene species. As described above, the C═C double bond is elongated to 1.49 Å whereby it begins to take on single bond character. A strong band, however, appears in the vibrational spectra at 1132 cm^{-1} which is attributed to CH_2 scissor mode. The calculation results indicate that this mode also contains a considerable fraction of C═C stretching character. The bands at 1380 and 1443 cm^{-1} were also found to have both C−C stretch and CH_2 bending character. Interestingly, there is a δ_{CH} peak which is present in the experiment at 1418 cm^{-1} which could not be found in the calculations on the π-bound state. This peak may be due to the presence of di-σ-species along with the π-bound intermediates on the surface as there are strong δ_{CH} modes in the calculated di-σ intermediate at 1379 and 1443 cm^{-1}. Comparisons of the

C−H stretching modes provide additional support for the possible presence of the di-σ-state or the interactions of ethylene with other surface species. The calculation results indicate that the bands attributed to C−H stretching frequencies were found to be shifted to lower frequencies due to the rehybridization about the carbon atom. This results from the stronger Pd−C bond that forms upon chemisorption in the di-σ-state. The experimental results show a broad spectrum that could easily cover both π- as well as di-σ-adsorption states. All of these results indicate that while the π-intermediate may be more favored on the surface, the di-σ-species is also likely to be present.

The energy of adsorption for ethylene via the di-σ-mode is −60 kJ/mol on the Pd_{19} cluster (and −62 kJ/mol on the Pd(111) slab) which is in excellent agreement with the value of −59 kJ/mol from low coverage temperature-program desorption experiments at ultrahigh vacuum conditions.[18] The predicted energy for the π-bound mode, −30 kJ/mol on the Pd_{19} cluster (and −27 kJ/mol on the Pd(111) slab), is also not very far off.

The comparison of TPD data with DFT calculation results suggests that the di-σ-mode is the favored adsorption state. Our analysis of the HREELS data however suggests that both π- and di-σ-species may be present on the surface. There are two likely explanations that may account for the difference between the implications derived from the calculated and the experimental results. The calculation results discussed so far deal only with the change in enthalpy between the di-σ- and π-adsorption states. Entropic considerations have been ignored. A closer examination of the optimized structures indicates that the π-bound ethylene mode has one additional degree of rotational freedom over the di-σ-state. In the π-bound mode, ethylene can easily rotate about the central C_{2v} axis that is coincident with the surface normal with very little change in its binding energy. The di-σ-bound ethylene, however, is locked to the surface via two σ-bonds and cannot rotate about this axis without breaking Pd−C bonds. This extra degree of freedom for the π-bound state leads to a change in the value of $T\Delta S$ of nearly 30−40 kJ/mol ($\Delta S/R \sim 4-5$ kcal/mol). This would indicate that the free energy change for the π- and di-σ-adsorption are nearly equivalent or that there is a slight preference for the π-bound mode. This would likely hold for the lower surface coverages. At higher surface coverages, however, ethylene would be locked into place due to repulsive interactions with little ability to rotate out of either the π- or di-σ-modes.

The second explanation concerning the differences between the experimental and theoretical predictions involves the assignment of the π- and di-σ-intermediates in the HREELS experiments. The distinction between the π- and di-σ-modes is difficult due to the coupling of C═C stretching and CH_2 bending modes as was discussed above. Stuve and Madix[19,20] have shown that ethylene on Pd(100) binds both π and di-σ. They recognized the difficulty in assigning the 1500 cm^{-1} and the 1290 cm^{-1} bands entirely to C═C stretch and CH_2 bending modes, respectively. Instead, they define what they termed the π/di-σ-parameter, which attempts to apportion the 1290 and 1500 cm^{-1} bands to C═C stretching and CH_2 bending modes and distinguish to what degree the or di-σ-modes are favored. The expression presented in eq 3 is calibrated based on Zeise salt and $C_2H_2Br_2$ as models for the and di-σ-models, respectively.[19]

$$\pi/\sigma(C_2H_4) = \frac{\left[\left(\frac{1623 - \text{band I}}{1623}\right) + \left(\frac{1342 - \text{band II}}{1342}\right)\right]}{0.366} \quad (3)$$

For systems which are primarily π-bonding, the π/σ-parameter should have a value between 0 and 0.38, whereas di-σ-bonding systems should be close to 1. By using the original HREELS data taken by Kesmodel and Gates,[16,17] the predicted value of π/σ-parameter is 0.45 which suggests that the π-bound mode is favored, but there is likely some di-σ-interactions as well. It is difficult to draw further conclusions based on the relative accuracy of the calculations as well as the difficulty in resolving the degree of coupling between C═C stretching modes and CH_2 angle bending modes from the experiments.

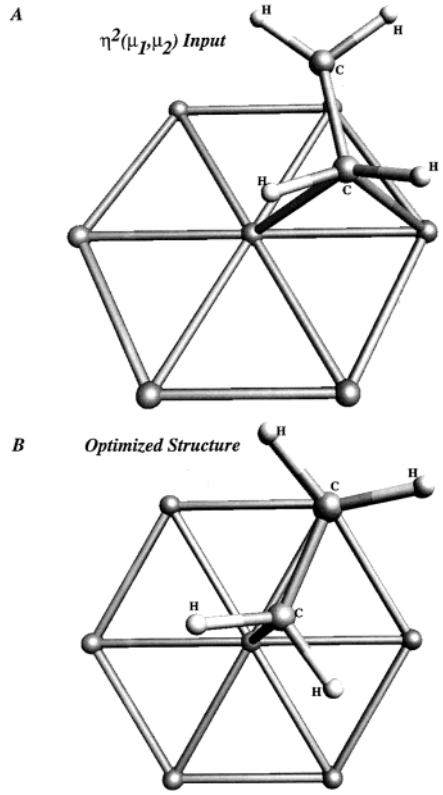

Figure 5. The di-σ η^2 (μ^1/μ^2)-adsorption of ethylene over a three-fold surface site. (A) The initial starting structure before optimization. (B) The optimized structure which indicates that ethylene moves from the 3-fold to the bridging di-σ-adsorption state.

Recent LEED analyses of ethylene on Pt(111) suggest a chemisorption state for ethylene that is characteristically different than the classical π- and di-σ-states shown in Figures 2 and 3. The mode is characterized as an π/di-σ-state with ethylene bound across a central 3-fold hollow site. Ethylene sits tilted with the respect to the surface which gives rise to both π- and di-σ-interactions.[7,8,22] In this arrangement, one of the carbon atoms sits atop a surface Pd atom while the other sits closer to the surface in a 2-fold bridge site. This could be characterized as a π/di-σ-interaction or as an $\eta^2(\mu^1,\mu^2)$ complex. To examine the likelihood of this adsorption state on Pd(111), we started with the structure depicted in Figure 5A. Upon optimization the ethylene rotated back to the more classical di-σ-configuration (Figure 5B) indicating the di-σ-adsorption state shown in Figure 3 is favored. Although the π/di-σ ethylene intermediate suggested by Cremer and Somorjai is not favorable, a π/di-σ vinyl species is. In recent work on the dehydrogenation pathways of ethylene, we found that the optimal structure for the vinyl intermediate involves a $\eta^2(\mu^1,\mu^2)$ interaction as is depicted in Figure 6. The CH_2 group prefers to sit atop a single metal atom center similar to the CH_2 group of the di-σ ethylene species. The CH group, however, is much more electron deficient and therefore prefers to sit directly across from the CH_2 site at the bridge site. The overall molecule resides above the 3-fold fcc

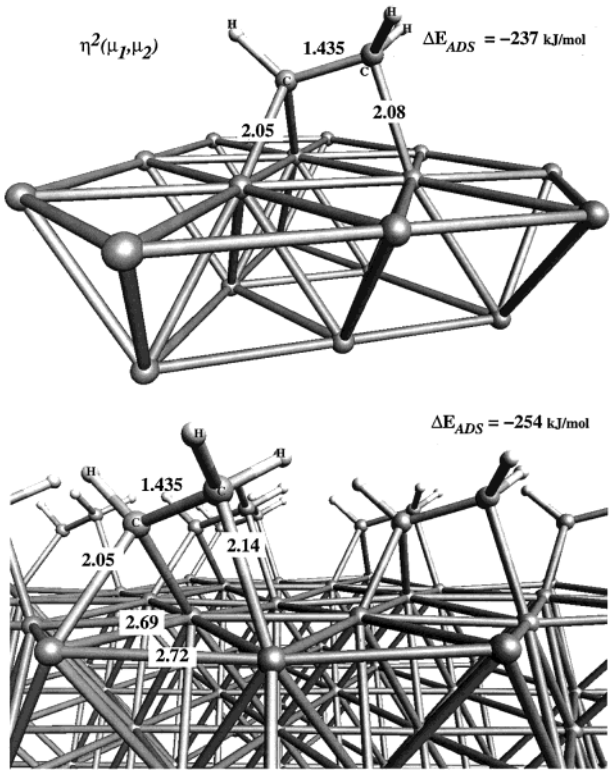

Figure 6. DFT-optimized structures and energies for the chemisorption of vinyl on model Pd(111) surfaces. The predicted chemisorption energies are (A) −237 kJ/mol on the Pd_{19} cluster model and (B) −254 kJ/mol for the ($\sqrt{3}$ *x* $\sqrt{3}$) *R*30° surface coverage on the 3-layer Pd slab model.

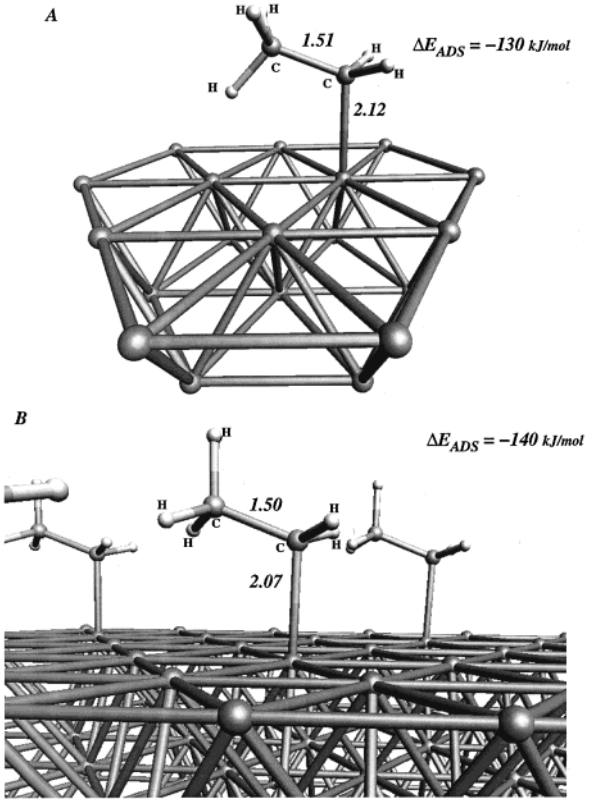

Figure 7. DFT-optimized structures and energies for the chemisorption of ethyl on model Pd(111) surfaces. The predicted chemisorption energies are (A) −130 kJ/mol on the Pd_{19} cluster model and (B) −140 kJ/mol for the (2 × 2) surface coverage on the three-layer Pd slab model.

site whereby its axis is tilted with respect to the metal surface. The predicted binding energy for vinyl on the Pd_{19} cluster was found to be −237 kJ/mol which is in good agreement with the computed value for −254 for vinyl in the (2 × 2) slab calculations. The bonding of this structure is consistent with LEED results[7,8,22] and could possibly be what was imaged rather than ethylene.

2. Coadsorption of Ethylene and Hydrogen. As a first step toward understanding the hydrogenation of ethylene, we examined the interaction between adsorbed ethylene and atomic hydrogen on a model Pd_{19} cluster of the (111) surface. Atomic hydrogen will sit at either the 2- or 3-fold hollow sites on the (111) surface. The lowest energy site for hydrogen was found to be the 3-fold fcc hollow. The lateral interaction between di-σ-bound ethylene and hydrogen was found to be 15 kJ/mol. Although the 3-fold bound hydrogen was found to be more stable, the lower energy reaction path was from the bridge site. This is consistent with the fact that the reaction is structure insensitive in that the bridge sites are essentially equivalent on different Pd surfaces. The overall reaction energy for the hydrogenation from the 2-fold site was found to be slightly exothermic at −3 kJ/mol.

Seigbahn[44] reported a lowering of the activation barrier of ethylene hydrogenation with respect to the *gas-phase ethylene* and metal−hydride complex. He also found a 71 kJ/mol increase in the binding energy of ethylene as the number of hydride ligands were increased from 1 to 2 over the single Pd complex. This would indicate an increase in the activation barrier from the *adsorbed ethylene* complex state. The situation on a metal surface, however, is significantly different due to the influence of neighboring metal atoms which share bonds with adsorbed hydrogen, thus dramatically reducing the direct electronic effects. The computed lateral interactions which are 15 kJ/mol are therefore weak.

3. Binding of the Ethyl Surface Intermediate. The first step in the Horiuti mechanism involves the addition of atomic hydrogen to adsorbed ethylene to form an ethyl surface intermediate. The ethyl (CH_3-CH_2*) species that is formed is one bond short of completing its valence shell. The missing C−H bond is compensated by the formation of a single M−C bond with the surface. This is consistent with the concepts derived from formal chemisorption theory and the ideas presented by Hoffmann,[39] Anderson,[23] and Whitten.[72] There is a balance between orbital overlap and Pauli repulsion which dictates the favored adsorption site.[52] Alkyl groups prefer the higher coordination sites for metals that lie to the left in the periodic table whereby donation and orbital overlap terms dominate the interaction. For metals that lie to the right, Pauli repulsion between the electrons in the filled states of the alkyl group and the greater number of electrons in the d-band dominate, thus leading alkyl groups to favor the atop adsorption sites.

The results shown here in Figure 7 indicate that the ethyl-surface interaction is relatively strong. The metal−adsorbate bond that forms helps to stabilize the electron deficient CH_3-CH_2 group. The optimized metal−carbon bond length was found to be 2.12 Å. The binding energy for an isolated ethyl intermediate on the Pd(111) surface is −130 kJ/mol from calculations on the Pd_{19} cluster. These results are in very good agreement with low coverage (2 × 2) periodic slab calculations which find an optimal M−C bond length of 2.07 Å along with a binding energy for the ethyl intermediate of −140 kJ/mol. As coverage is increased, there are weak repulsive interactions between the methyl groups on neighboring ethyl intermediates.

Ethyl adsorbed at a bridge site was found to be −75 kJ/mol which is 55 kJ/mol less stable than that bound atop a metal center.

4. Low Coverage Reaction Coordinate Analyses. a. Hydrogenation of the Di-σ Bound Ethylene. At low pressures, the first hydrogen addition step in the Horiuti mechanism is typically thought to be the rate-determining step in the cycle.[75,76] Fundamental UHV studies are limited in their analysis of hydrogenation, because at ideal vacuum conditions, hydrogen prefers to desorb before reacting with surface hydrocarbon intermediates. There is, however, a wealth of UHV studies on the reverse reaction step, the oxidative addition or C−H bond activation of alkyl intermediates over metal centers and surfaces.

i. The Reverse Reaction: Oxidative Addition. We present our result first in terms of the reverse reaction, oxidative addition (C−H bond breaking), so that we can compare them against well-defined low coverage UHV analyses. The activation of surface alkyl intermediates has been examined in detail under UHV conditions by Gellman,[73] Bent,[11,74] Zaera,[12,24,75,76] and others. The mechanism involves a β-hydride elimination as was suggested by Gellman[73] for the activation of alkyl intermediates on Cu. Gellman[73] found that when an electronegative substituent such as a fluorine atom is attached to the β carbon position the intrinsic activation barrier is increased. Electron-withdrawing substituents increase the partial positive charge (or reduce the negative charge) on the β-carbon. This destabilizes the transition state with respect to the reactant state. Bent[11,74] found further evidence for β-hydride elimination and suggested that the transition state takes on a syn conformation. HREELS experiments along with the results of different sterically hindered olefins, suggested that the transition state is either a three-center (M−C−H) or a four-center (M−C−H-M) cyclic complex.

The reaction coordinate for the oxidative addition of ethyl to form ethylene and hydrogen was determined by calculations on both the Pd_7 and the Pd_{19} clusters. A rough potential energy surface was constructed by performing a series of constrained optimizations along the chosen reaction coordinate, which involves the C−H stretching mode. At each given point along the two-dimensional potential energy surface, the C−H bond was fixed while all other structural variables were allowed to optimize. The potential barrier for this path occurred at a C−H stretch of 1.7 Å. A complete frequency analysis was then performed on this approximate transition-state structure. The negative eigenmode which corresponds to the saddle point on the PES was identified. This state was subsequently used in a more rigorous mode following technique to isolate the "true" transition state. The resulting structure along with the force vectors that identify the actual reaction coordinate that connects the reactant and product states are depicted in Figure 8.

Intrinsic activation barriers are measured with respect to the *adsorbed ethylene reference state*. The barrier predicted for β C−H activation of ethyl to ethylene and hydrogen on Pd_7 was +59 kJ/mol. DFT predicted energies, however, are known to be much more sensitive to cluster size variations than geometric structures or frequencies. To provide a more accurate account of the activation energy, the transition state that was found on the Pd_7 cluster was used as a starting point to isolate the barrier on the Pd_{19} cluster. The predicted activation energy over the Pd_{19} complex was found to be +69 kJ/mol which is slightly higher than that computed on the Pd_7 cluster. The results for the initial ethyl reactant, the transition state and the surface ethylene and hydrogen product are depicted in Figure 9. The overall reaction energy for ethyl to ethylene and hydrogen over Pd_{19} was −3 kJ/mol. To help confirm the cluster activation barriers we performed calculations on the three-layer Pd(111) slab using a (2 × 3) supercell. The barrier for C−H bond activation was calculated to be +63 kJ/mol which is in excellent agreement with the cluster results of +69 kJ/mol. The structure of the transition state complex on the Pd(111) slab was essentially identical to that found on the Pd_{19} cluster. These results are also consistent with experimental values reported for ethyl activation over Ni and Pt which range from 40 to 60 kJ/

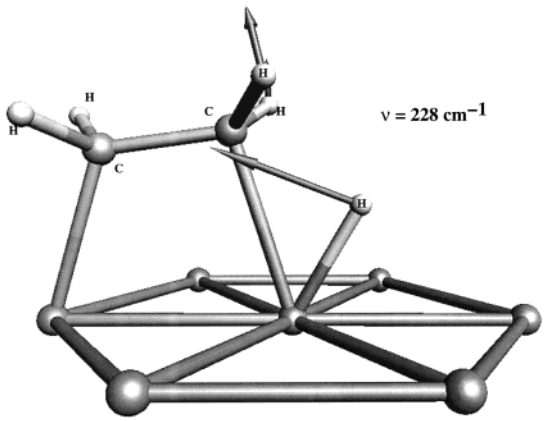

Figure 8. The isolated transition state structure for the activation of the ethyl C−H bond over the model Pd_7 cluster. The vectors correspond to the motion along the reaction coordinate. There is motion along the primary C−H stretch as well as secondary movement of the neighboring C−H groups which illustrates the change from sp_3 to sp_2 bonding at the carbon center. The negative eigen mode associated with the transition state appears at −228 cm^{-1}.

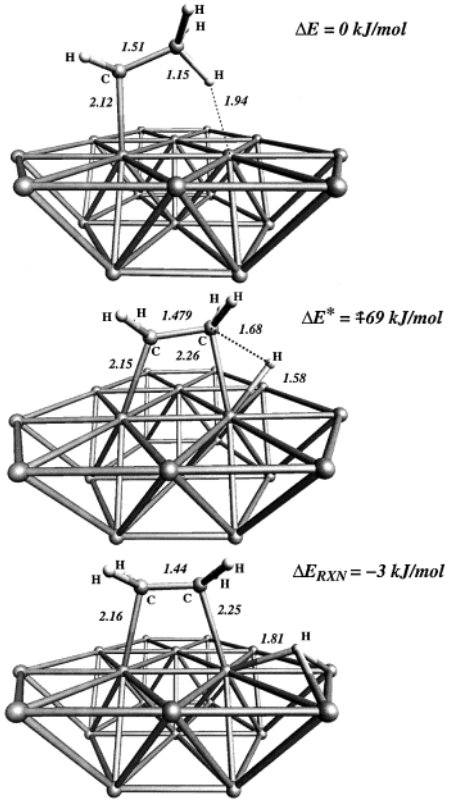

Figure 9. The activation of the C−H bond of adsorbed ethyl at low surface coverage to form surface ethylene and hydrogen over the Pd_{19} cluster. The reactant, transition and product states for this reaction are depicted in (A), (B), and (C), respectively. The energies are reported relative to the initial reaction state. The reverse reaction which involves the hydrogenation of di-σ-bound ethylene to ethyl has a barrier of +72 kJ/mol and is endothermic by 3 kJ/mol.

mol.[11] Kovács and Solymosi[77] measured the barrier to be between 40 and 60 kJ/mol from UHV TPD studies of ethyl iodide on Pd(100).

The structures of the transition state complexes for both cluster and slab models are essentially the same. The transition state complex on the Pd_{19} cluster is shown in the middle panel of Figure 9. There is a substantial elongation of the β C−H bond before it begins to interact with the metal surface. This agostic C−H stretch is characteristic of other C−H activation steps over homogeneous metal centers.[43,76] C−H activation involves the transfer of charge from the metal surface into the antibonding σ_{C-H}*-orbital. The σ_{C-H}*-state, however, is fairly high in energy. A significant stretch in the C−H bond is therefore required before the σ_{C-H}*-state becomes low enough in energy to accept charge transfer from the surface. The back-donation of charge from the surface into the antibonding σ_{CH^*}-orbital subsequently promotes C−H bond scission. This is a late transition state whereby the activated complex looks to be much more "product-like". In addition to the long C−H bond, both metal−hydrogen and metal−carbon bonds begin to form in-order to stabilize both the hydrogen and carbon fragments from the activated methyl group. These results are consistent with the ASED results of Anderson[23] which examined the activation of C−H bond of adsorbed ethyl on Pt(111). The transition state also looks quite similar to those found for methane activation by van Santen,[78−79] Whitten,[80,72] Siegbahn,[81,82] and Nørskov.[83] There is one notable exception. In the activation of the surface ethyl intermediate, the CH_2 group of the ethyl reactant is already attached to the surface, thus limiting its mobility. We have also found that the general features of the activated complex discussed here apply to other C−H bond activation steps such as that for the activation of the methyl groups of surface acetate.[84] An analysis of the change in the atomic charges as the reaction is carried out from the reactant, transition, and product states indicate that as the C−H bond is broken, the charge on the carbon increases. Hydrogen appears to transfer as a hydride. Both of these features are consistent with the views presented by Gellman.[73]

The reverse process, ethylene hydrogenation over Pd, was determined from microscopic reversibility. The overall reaction energy for hydrogen addition to ethylene (reductive elimination of ethylene) in the absence of any lateral interactions was found to be endothermic by +18 kJ/mol. When ethylene and hydrogen sit at nearest neighbor sites whereby they share bonds with the same metal atom, they are weakly repulsive (+15 kJ/mol) with one another. This lowers the overall endothermicity of this reaction to +3 kJ/mol (as seen in Figure 9). The intrinsic barrier for this first hydrogen addition step was found to be +72 kJ/mol with respect to the reactant state where hydrogen and ethylene share a metal atom neighbor. The intrinsic barrier is increased to +87 kJ/mol if it is measured with respect to the *isolated* ethylene and atomic hydrogen surface fragments. The difference in these values is attributed to the repulsive interactions when ethylene and hydrogen share metal atoms (+15 kJ/mol). The activation barriers and overall energies for all the reaction steps considered in this work are reported in Table 4.

b. Hydrogenation of the π-Bound Ethylene. The hydrogenation of π-bound ethylene is more complicated in that the expected reaction coordinate is thought to involve the "slip" of the π-bound ethylene across the metal atom to which it is bound to allow the hydrogen to insert into the bond between carbon and the metal.[44] This was shown schematically in Chart 1 depicted earlier. The central M-CH_2−CH_2−H complex that forms allows hydrogen to transfer from the metal to ethylene.

TABLE 4: DFT-calculated Activation Barriers and Overall Reaction Energies for the Hydrogenation of Ethylene to Ethyl and the Hydrogenation of Ethyl to Ethane over Different Model Pd(111) Surfaces[a]

	$C_2H_4^* + H^* \rightarrow C_2H_5^*$		$C_2H_5^* + H^* \rightarrow C_2H_6(g)$	
	forward	reverse	forward	reverse
		Pd_{19}		
$\theta = 0$				
di-σ				
ΔE^*	+72	+69	+71	+105
ΔE_{rxn}	+3	−3	−35	+35
			(without lateral interactions)	
		Pd(111) Slab		
$\theta = 0.25$				
di-σ				
ΔE^*	+87	+63		
ΔE_{rxn}	+18	−22		
$\theta = 0.60$				
di-σ				
ΔE^*	+82			
ΔE_{rxn}				
π				
ΔE^*	+36			
ΔE_{rxn}	−18			

[a] All reported activation energies are intrinsic barriers which were calculated from the adsorbed state. The reverse barriers for ethyl and ethane C−H bond activation are also reported. Increasing the coverage leads to a change in the site that is most active for hydrogenation. At low coverages ($\theta = 0-0.25$) the reaction proceeds through the di-σ-adsorption state. At higher coverages, the barrier to hydrogenate π-bound ethylene is significantly lower than that for di-σ ethylene.

We used the structure reported by Seigbahn[44] for ethylene hydrogenation over Pd_1H_2 as a first guess for our calculations on both the Pd_{19} cluster and the periodic Pd(111) slab. At low surface coverages, the repulsive interactions that take place between hydrogen and ethylene in traversing from the reactant state toward the transition state actually push ethylene from its π-bound site to the energetically more favored di-σ-state. This is shown in Figure 10. At low coverages, there appears to be no direct channel to hydrogenate from the π-bound state. Ethylene will only react under these conditions from the di-σ-state. The π-bound state is simply an intermediate that must first be converted to the di-σ-species before it will hydrogenate.

c. Hydrogenation of Surface Ethyl to Ethane. The second step in the hydrogenation of ethylene to ethane involves the addition of atomic hydrogen to the adsorbed ethyl surface intermediate. The barrier for this step is thought to be lower than that for the addition of the first hydrogen to form the ethyl intermediate. We again start by analyzing the reverse elementary reaction step which involves the activation of a C−H bond of ethane. The isolated transition state which is shown in Figure 11 is very similar to what we found for the activation of ethyl* to ethylene*. The calculated barrier required to activate ethane to form surface ethyl and surface atomic hydrogen was calculated to be +106 kJ/mol. This is consistent with the values in the literature for methane activation over Ni.[83] The transition state is relatively late with respect to the C−H bond stretch (1.51 Å). The basic structure of the activated complex involves a three-center M−C−H intermediate. As the C−H bond is broken, both M−C and M−H bonds are formed. The overall reaction energy for ethane activation to surface ethyl and hydrogen was calculated to be endothermic by +35 kJ/mol. Much of this, however, (30 kJ/mol) is due to the repulsive interactions that result when an adsorbed ethyl and an adsorbed hydrogen share a metal atom center.

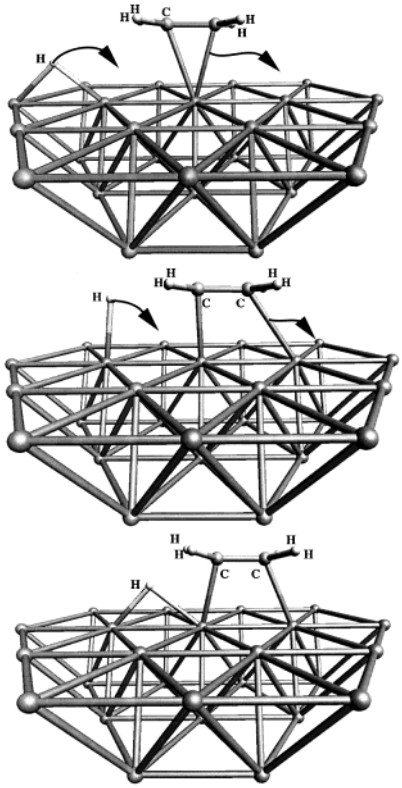

Figure 10. A sequence of steps that show the path of the -ethylene as hydrogen at low surface coverage. The repulsive interactions between the π-bound ethylene and the approaching hydrogen are minimized as ethylene moves from the π-bound state to the di-σ-state.

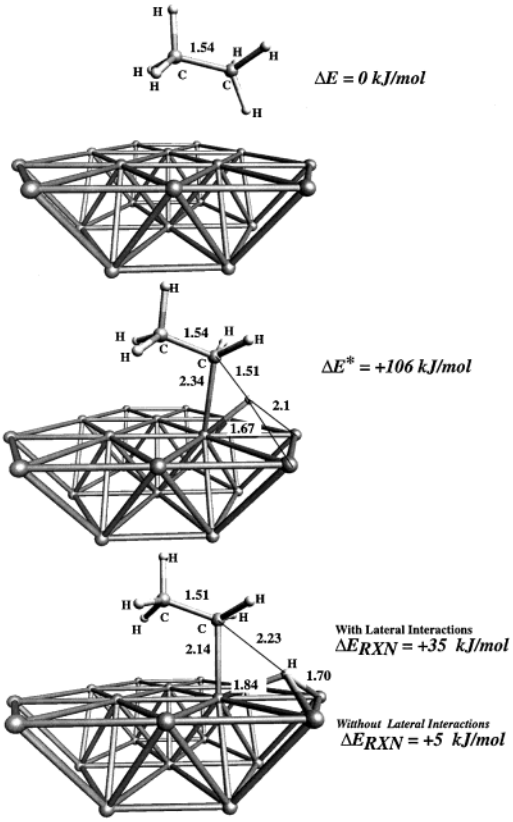

Figure 11. The C−H bond activation of ethane over Pd(111) to surface ethyl and hydrogen intermediates. The reactant, transition, and product states for this reaction are depicted in (A), (B), and (C), respectively. The activation barrier for C−H activation barrier (+106 kJ/mol) and the overall reaction energy (+5 kJ/mol) were computed with respect to the reactant state (ethane/Pd_{19}). This reaction is the microscopic reverse of hydrogen addition to surface ethyl to form ethane which has an activation barrier of +71 kJ/mol and is exothermic by 35 kJ/mol.

The predicted barrier for the *hydrogenation* of ethyl to ethane (the reverse path) is +71 kJ/mol which is about the same as that for the hydrogenation of ethylene to surface ethyl. The overall hydrogenation reaction energy is exothermic by −35 kJ/mol from the state where both ethyl and hydrogen share a metal atom center. If, however, we assume that the surface ethyl and hydrogen do not interact on the surface, then the overall reaction energy is −5 kJ/mol. The first hydrogenation step of ethylene to ethyl was found to be endothermic by +3 kJ/mol. The difference between the two is likely due to the stability of the final ethane product. The overall energy of the reaction for ethylene hydrogenation to ethane was found to be −158 kJ/mol which is in reasonable agreement with the experimental value of −137 kJ/mol.

The results above indicate that the hydrogenation of ethylene *at low coverages* primarily proceeds via the di-σ-bound ethylene intermediate. Although the π-bound state is present it does not appear to be active in hydrogenation. The π-bound state does however appear to be a precursor to the reactive di-σ-state. The energies computed for the sequence of elementary reaction steps at low coverage are summarized in the potential energy diagram depicted in Figure 12. Ethylene adsorbs in both the π- and di-σ-adsorption states. Hydrogenation, however, proceeds only through the di-σ-bound intermediate (step1). Hydrogen dissociates over Pd to form two surface hydrogen atoms which subsequently react with surface ethylene and ethyl. H_2 dissociation over Pd(111) was found to be exothermic releasing 104 kJ/mol (step 2). The intrinsic activation barrier for the reaction of ethylene and surface hydrogen was +72 if the reference reactant state is the ethylene-hydrogen complex which share metal atoms. If, however, we take isolated ethylene and hydrogen as the reactant state, then the barrier is slightly higher at +87 kJ/mol. This is due to the fact that we remove the weak lateral repulsive interactions (+15 kJ/mol) which take place when ethylene and atomic hydrogen share a metal surface atom. This is shown as a separate step (step 3) in Figure 12. At low surface coverages, however, the *apparent activation barrier* is measured with respect to the *gas phase state* rather than the *adsorbed surface state.* At lower coverages, the surface coverage of ethylene is assumed to be less than the fraction of vacant sites (that is $1 \gg K_{\text{ethylene}}P_{\text{ethylene}}$ in a Langmuir−Hinshelwood model). The rate, therefore, is proportional to $kK_{\text{ethylene}}P_{\text{ethylene}}$. The apparent rate that is measured with respect to changes temperature should change as $E^{a}_{\text{app}} = E^{a}_{\text{intrinsic}} - \Delta H_{\text{ads.}}$ The adsorption energy and the activation barrier compete with one another. The measured or apparent activation barrier, therefore, is that which is measured with respect to the gas phase. In this case, the heat of adsorption of ethylene acts to lower the intrinsic reaction barrier. The apparent barrier is calculated to be +27 kJ/mol. Since the barrier is measured with respect to the gas phase lateral interactions are not involved. The overall reaction energy for the first surface hydrogenation step is slightly endothermic at +3 kJ/mol (step 4). The subsequent hydrogenation of ethyl to form ethane (step 5) is exothermic by 5 kJ/mol (step 5). The overall energy for the reaction of

$$\text{ethylene(g)} + 2\text{H}_2\text{(g)} \rightarrow \text{ethane(g)}$$

is calculated to be exothermic by −158 kJ/mol. The value estimated from thermochemical estimates is −140 kJ/mol.

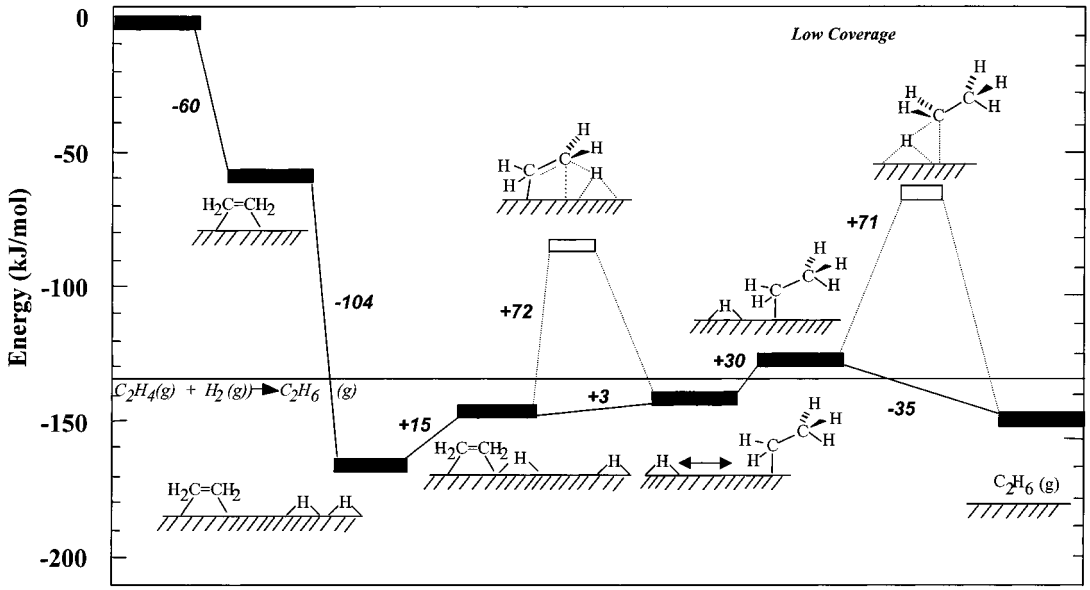

Figure 12. The overall potential energy diagram for ethylene hydrogenation over Pd(111) at low surface coverages. The solid boxes refer to reactant, intermediate, and product states, whereas the two white boxes denote the transition state structures and energies for the surface reactions of ethylene to ethyl and ethyl to ethane.

B. High Coverage Chemisorption and Reaction Path Analyses. The results presented so far provide the picture for what happens on the pristine low coverage Pd(111) surface. It is well established that the relative abundance of different surface species and their role in the mechanism can change as the pressure and hence the surface coverage are increased to mimic actual reaction condition. Below we examine the effects of higher surface coverages of ethylidyne, atomic carbon, oxygen, and hydrogen on chemisorption and hydrogenation reactivity.

1. The Role of the Ethylidyne Intermediate. Both low pressure surface science as well as higher pressure fixed-bed reactor studies indicate that ethylidyne is present to a significant extent on Pd and Pt under reaction conditions. Ethylidyne is the primary decomposition product of ethylene and is taught only to be a spectator species.[6,8,9,22] The results of cluster and slab calculations indicate that the binding energy of ethylidyne at the 3-fold fcc site on Pd(111) is −620 and −636 kJ/mol, respectively. The optimized structures for ethylidyne on the Pd_{19} cluster and the 3-layer Pd slab are shown in Figure 13. The calculated binding energy is a strong function of the reference state that is chosen for gas-phase CH_3-C intermediate. We have taken the gas-phase ethylidyne intermediate to be a quartet state with three unpaired electrons as it mimics its structure on the surface. The more stable ground-state energy for the CH_3C intermediate, however, involves the pairing of two electrons to form a doublet state. The ethylidyne adsorption energy with respect to the lower energy doublet state is 125 kJ/mol weaker at −511 kJ/mol. Regardless of which state is used, the binding energy is still very strong. The optimized C−C bond length for ethylidyne on Pd was 1.50 Å which begins to approach the C−C bond of ethane. This leads to a relaxation of the palladium atoms that make up the surface−adsorbate complex out of the surface by about 0.12 Å. The interlayer spacing between the metal surface atoms involved in the adsorption complex and those in the second layer of the surface are relaxed from 2.75 to 2.88 Å. This is very similar to the results found by Somorjai [85] who report from LEED studies a relaxation of the surface layer of about 0.1 Å for ethylidyne on Pt(111). Once again, results from the cluster and slab calculations were found to be essentially the same with energy difference of 16 kJ/mol (Figure 13A,B).

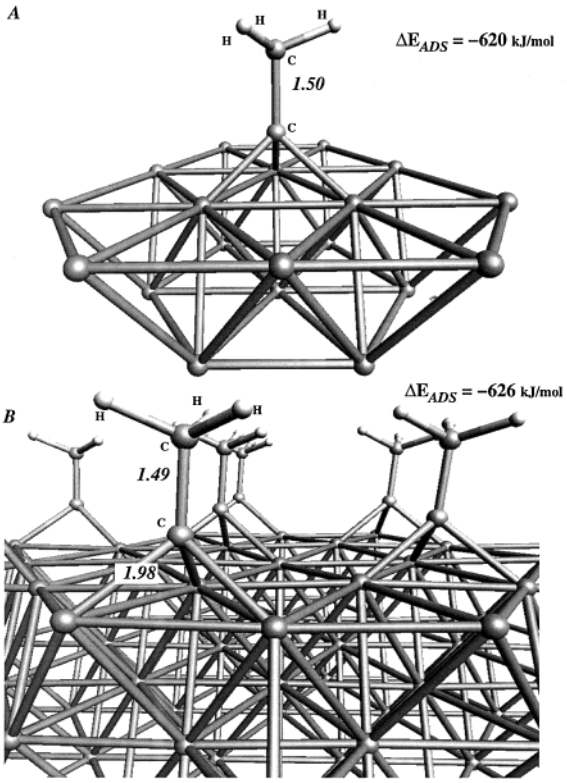

Figure 13. DFT-optimized structures and energies for the chemisorption of ethylidyne on model Pd(111) surfaces. The predicted chemisorption energies are (A) −620 kJ/mol on the Pd_{19} cluster model and (B) −636 kJ/mol for the 2 × 2 surface coverage on the three-layer Pd slab model. These values are derived using the quartet reference state for ethylidyne. The more stable gas-phase reference state for ethylidyne is that of the doublet. The adsorption energy found using the doublet reference state was −511 kJ/mol.

The surface diffusion of ethylidyne was modeled by calculating the chemisorption energies of ethylidyne at the stable 3-fold fcc and hcp sites which serve as the reactant and product states, respectively. The transition state for this path is taken to be

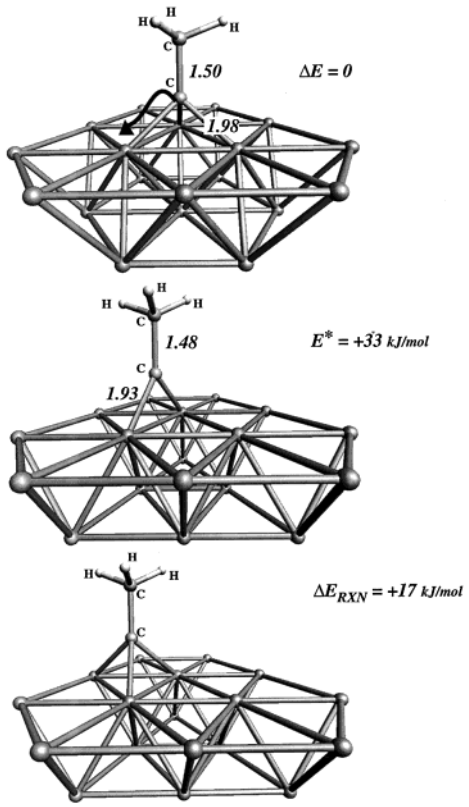

Figure 14. The diffusion of ethylidyne from the fcc 3-fold adsorption site to a neighboring hcp 3-fold site over the Pd_{19} cluster. The reactant (fcc), transition (bridge) and product (hcp) states for the diffusion of ethylidyne are depicted in in (A), (B), and (C), respectively. The energies reported are relative to the initial reaction fcc state.

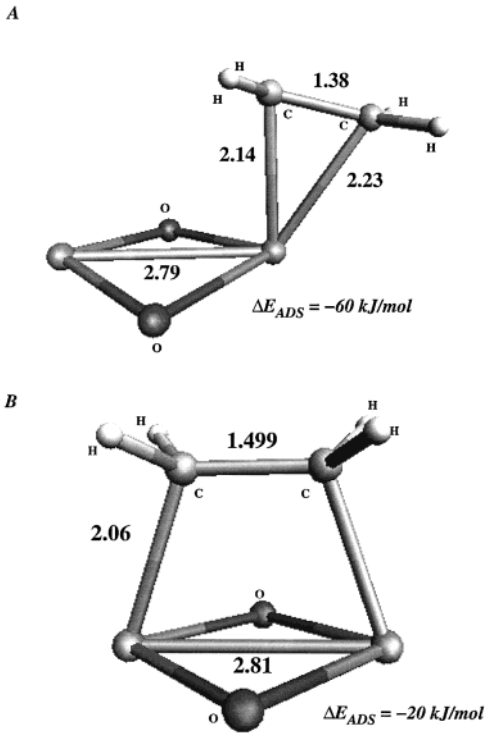

Figure 15. The effect of metal oxidation state on the modes and energy of ethylene chemisorption. The binding energy on the bare Pd_2 cluster was found to be similar to that for ethylene on periodic slab and Pd_{19} cluster with a value of about −60 kJ/mol (di-σ) and −30 kJ/mol (π). On the Pd_2O_2 cluster, the energy for the π-bound ethylene is increased by 30 kJ/mol whereas the binding energy for the di-σ-state is reduced by 40 kJ/mol. On these partially oxidized Pd clusters, the π-bound mode is favored.

ethylidyne at the bridge site which connects the fcc and hcp sites. The calculated reactant, transition, and product states are shown in Figure 14. The binding energy of ethylidyne at the bridge site (−593 kJ/mol) was found to be slightly weaker than that at the fcc site (−636 kJ/mol). The estimated barrier for ethylidyne surface diffusion is therefore fairly low at +33 kJ/mol. The overall energy to move from the fcc to the hcp site was only +17 kJ/mol. The low barrier for ethylidyne surface diffusion is consistent with surface science results as well as the extended Hückel (ASED) calculations performed by Anderson[21] which indicate that surface ethylidyne species are quite mobile.

Ethylene is thought to readily convert to ethylidyne on supported Pd particles.[6,86] The conversion of ethylene on Pd(111) however is thought to be significantly lower.[87−89] This is most likely due to the presence of unsaturated defect sites on the supported particles as compared to the well-defined Pd(111) surface. Dumesic et al.[90] have recently performed microcalorimetric experiments for ethylene adsorption over Pd/SiO_2. They found that ethylene liberates 220 kJ/mol of heat when it is adsorbed on particles with coverages less than 1%. This heat release decreases to −170 kJ/mol as the surface coverage is increased to about 1%. The value falls even further to −145 at coverages of about 8%. They speculate that the heat release is due to possible surface reactions of ethylene which involve the formation of ethylidyne or other hydrocarbon intermediates. The energies that we find here for the reaction of ethylene to CH_3C^* and H*, however, would only release about 10 kJ/mol. Breaking the C−C bond, on the other hand, would release 150 kJ/mol which is in reasonably good agreement with the microcalorimetric experimental results. This is also consistent with the fact that hydrogenolysis is structure sensitive whereas C−H bond formation is not.

2. The Effects of Coadsorbed Oxygen and Carbon. As was indicated, the working surface of an ethylene hydrogenation catalyst may contain considerable amounts of ethylidyne and other hydrocarbon intermediates which can significantly affect chemisorption and surface reactivity. In an effort to probe these interactions we carried out a series of calculations in the presence of atomic oxygen and carbon.

The influence of oxygen on the chemisorption of ethylene depends on the ethylene adsorption mode, the surface coverage, as well as the specific local bonding configuration of ethylene and oxygen. We carried out a series of calculations on small Pd_2O_x clusters as well as larger Pd(111) slabs in an effort to distinguish between the effects of changing the local oxidation state at specific metal centers and through-space repulsive interactions. The adsorption of ethylene in the presence of surface oxygen reveals that the π-bound mode is favored over the di-σ-mode. Both geometric and electronic factors appear to contribute. This was first examined by exploring the adsorption of ethylene on small Pd_2O_x complexes. The results for ethylene adsorption on Pd_2O_2 as compared to Pd2 are shown in Figure 15. The binding energy for ethylene sitting in the π- and di-σ-modes on the naked Pd_2 structure were found to be very close to those calculated for the adsorption on larger Pd_{19} clusters and Pd slabs. Two oxygen atoms were subsequently added to the bridge sites of the Pd_2 cluster. This increased the binding energy of the π-bound mode from −25 to −60 kJ/mol while decreasing that for the di-σ-bound mode from −60 kJ/mol to −20 kJ/mol. A closer analysis of the electron density indicates

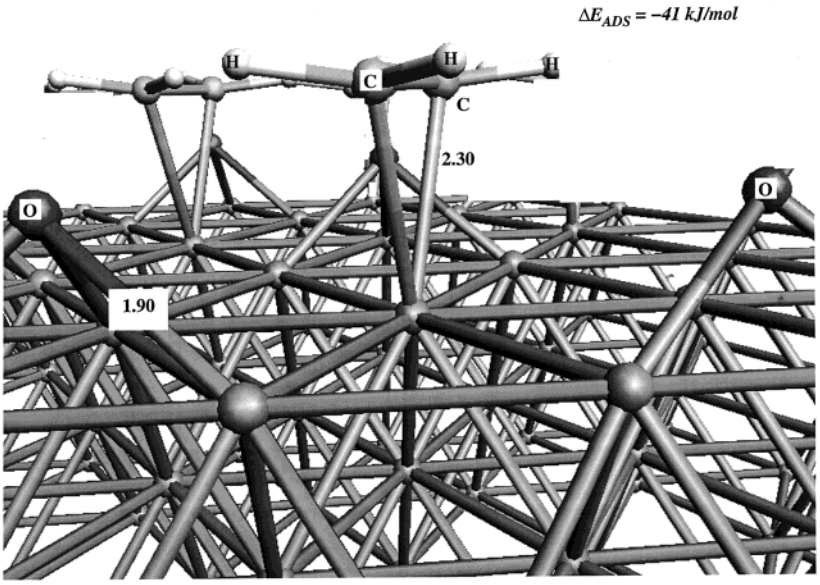

Figure 16. Coadsorption of ethylene and oxygen in a (2 × 2) surface structure. In this particular configuration, the ethylene and oxygen do not share metal atoms and the chemisorption energy is increased by 11 kJ/mol from the low coverage ethylene results. The predicted adsorption energy for ethylene is −41 kJ/mol.

that charge is transferred from the Pd to oxygen, thus inducing a partial positive charge on the Pd centers. This decreases the degree of back-donation which favors the π-mode over the di-σ-mode. Oxygen, however, prefers to sit in the plane to maintain a square-planar arrangement around the Pd centers of the Pd_2O_2 complex. This also reduces the through-space repulsive interaction that exist between ethylene and oxygen. The end result is that as palladium becomes partially oxidized the π-bound adsorption becomes stronger and begins to dominate over di-σ-adsorption which becomes weaker. The increase in the binding energy for the π-bound adsorption state of ethylene as Pd becomes more oxidized is consistent with results reported by Seigbahn[44] which show an increase of over 71 kcal/mol as the number of hydride ligands on the PdH_x are increased from 1 to 2.

On a metal surface, however, the effects of oxygen are more complicated. Oxygen no longer has the freedom to move into the surface plane to avoid direct interactions with ethylene. If oxygen and ethylene share metal atoms the interaction is repulsive. This is due to the direct repulsive interaction between the oxygen and ethylene that occur through space. These repulsive interactions dominate any enhancement due to partial changes in the oxidation state of the metal. If, however, oxygen and ethylene are moved apart and sit at *nearest-neighbor* sites such as shown in Figure 16, they are weakly attractive. Lateral surface interactions act to increase the binding energy of ethylene in the π-bound state from −30 to −41 kJ/mol. The interactions, between di-σ ethylene and coadsorbed oxygen, however, are always repulsive. For a (2 × 2) surface coverage, π-bound ethylene and 3-fold O/Pd(111) do not share any surface metal atoms. This, however, is not possible for the di-σ-state (at a (2 × 2) coverage), which requires two surface atoms to bind to, and therefore introduces repulsive interactions due to sharing of metal atoms. Stuve and Madix[20] found a similar shift from the di-σ- to π-modes when ethylene was adsorbed in a 0.25 ML coverage on the Pd(100) surface. It is well established that there is charge transfer from the metal to the more electronegative adsorbates such as oxygen, carbon, nitrogen, and sulfur. Vannice et al.[91] discussed similar ideas in explaining the changes in the adsorption of ethylene on supported platinum particles. They indicate that either geometric or electronic factors may govern this change in adsorption site favorability but were unable to discriminate between the two. We also find that both factors are important. At low to moderate coverages, oxygen weakens the di-σ-interaction while strengthening that of the π mode. This inevitably leads to differences in site occupation as the number of sites are decreased due to higher surface coverages of oxygen. In addition, we see that charge transfer to the oxygen helps to stabilize the π-bound species. These results appear to be consistent with experiments as well as the analysis presented by Stuve and Madix.

At higher coverages, however, whereby ethylene and oxygen begin to share metal atoms, the through-space repulsive interactions begin to dominate and both the and di-σ-modes of ethylene are weakened. If ethylene and oxygen share a single metal atom, then the repulsive interactions decrease the π-bound and di-σ-binding energies to −20 and −40 kJ/mol**,** respectively. At these higher coverages, the structure of di-σ-adsorbed ethylene is remarkably similar to that of the π-bound ethylene intermediate at lower coverages. The Pd−C bond and C═C bonds at higher coverages are now 2.3 and 1.38 Å. This would indicate that their vibrational frequencies would likely resemble that of the π-bound ethylene structure.

We find very similar results when ethylene is adsorbed on surfaces covered with carbon. This analysis more closely mimics the surface under working reaction conditions where a fair amount of surface carbon intermediates exist. Our results indicate that the presence of carbon on the surface can, in some circumstances, decrease the ethylene adsorption energy, whereas, it can increase it in others. When ethylene and carbon directly share metal atoms, the *through-space* repulsive interactions dominate and the interactions are repulsive. If they are separated by a single metal bond, the *through-surface* interactions increase the stability of ethylene in the π-bound mode. In the di-σ-mode, the interactions are predominantly repulsive, thus weakening the ethylene adsorption in the di-σ-mode. These interactions can be quite important not only in changing the stability of the intermediates but also in altering the kinetics. Our recent results from Monte Carlo simulation show these features can begin to control measured reaction rates.[27]

3. High Coverage Reaction Path Analyses. Adsorbate−adsorbate interactions not only change the energy of adsorption

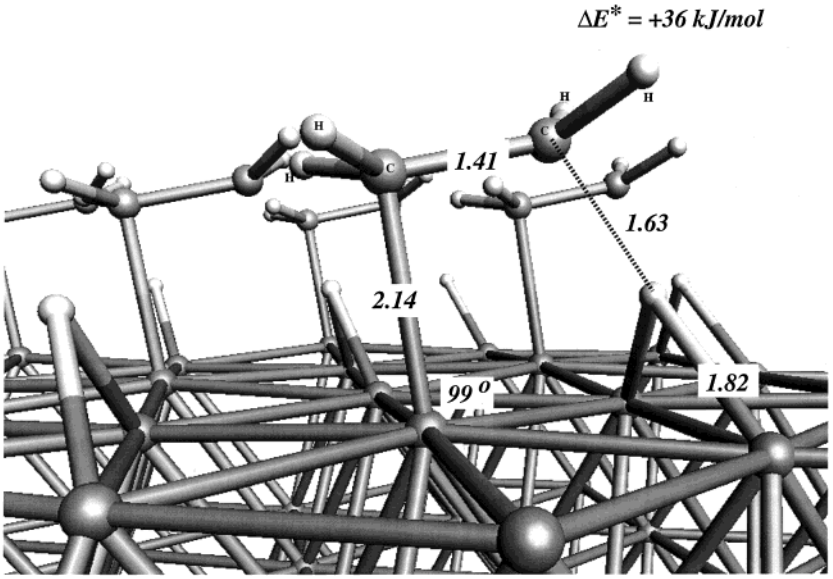

Figure 17. The isolated transition state for ethylene hydrogenation from the π-bound mode at the higher surface coverages (0.6 ML) of the ($\sqrt{3}$ x $\sqrt{3}$) *R*30° coadsorbed ethylene hydrogen system.

but can also significantly alter the activation barriers as well as the reaction selectivity. This is governed by the change in the strength of the metal−adsorbate surface bonds as the coverage is increased. To examine higher coverage situations, we placed both ethylene and hydrogen in ($\sqrt{3} \times \sqrt{3}$) *R*30° structures on the Pd(111) surface. This results in a surface saturation of 0.6 ML. We subsequently probed the activation barriers for hydrogen addition to both the π- and di-σ-adsorption states.

These higher coverages were found to have only a very minor effect on the *intrinsic activation barrier* for hydrogenation of ethylene from the di-σ-mode. The activation barrier at higher coverage is reduced by only 5 kJ/mol from +87 to +82 kJ/mol from that the low coverage state. Although the effect on the *intrinsic barrier* was small, the change in the *apparent barrier* was much greater. At higher coverages, the apparent barrier is equivalent to the intrinsic barrier and is therefore measured with respect to the *adsorbed surface state*. At low coverages, however, the apparent barrier is measured with respect to the *gas phase*. This involves subtracting the reactant's adsorption energy from the intrinsic barrier. Our calculations for ethylene hydrogenation from the di-σ-adsorption state at 0.6 ML coverage indicate that the intrinsic activation barrier is +82 kJ/mol which is equivalent to the apparent barrier at high coverages. At the lowever coverages discussed earlier, we found that the intrinsic barrier was 87 kJ/mol while the apparent barrier was 27 kJ/mol.

For the π-bound state, however, we find that the increase in surface coverage leads to a significant decrease in the intrinsic activation barrier as it falls to only +36 kJ/mol. This is favored by 46 kJ/mol over the barrier for the di-σ-state. Early we showed that at *low surface coverages*, the hydrogenation from the π-bound state does not occur. At low coverage, the repulsive interactions which arise as hydrogen is brought toward a π-bound ethylene, push ethylene from its atop π-bound site into the di-σ-site. At higher surface coverage, ethylene is much more likely to exist as a π-bound intermediate than as a di-σ-species in order to reduce some of the repulsive interactions. The repulsive interactions that exist at higher coverages will either drive ethylene off the surface or lower its activation barrier. Indeed, at 0.6 ML, the neighboring adsorption sites were shutdown due to the presence of coadsorbed hydrogen. Ethylene is therefore "pinned" at the π-bound adsorption site. Ethylene and hydrogen subsequently react via a "slip" type mechanism as is shown in Figure 17. The isolated transition state was found to be different than that for the classical "slip" mechanism reported by Hoffmann and Seigbahn over homogeneous Pt and PdH_2 clusters (see Chart 1). The classical complex depicted in Chart 1 was examined but found to be unfavorable on the metal surface. There is a considerable level of steric crowding about the active metal atom center. The angle between ethylene and hydrogen are constrained due to the presence of the metal surface. The predicted barrier for this transition state was found to be over 120 kJ/mol. The metal surface, however, can help to stabilize the transition state if the ethylene−hydrogen reaction ensemble is allowed to spread out over neighboring metal atoms. This avoids steric crowding and enables both ethylene and hydrogen fragments in the transition state to interact with the surface. The isolated transition state for this reaction is depicted in Figure 17. Three metal atoms participate in stabilizing the activated complex. The potential energy surface for ethylene hydrogenation to ethyl at high coverage from the π-bound state is shown in Figure 18. The barrier for this π-bound state at higher coverages was found to be only +36 kJ/mol which is considerably less than that for the hydrogenation from the di-σ-state at higher surface coverages. This indicates that at higher coverages the π-bound state becomes the key reactive intermediate. These results are consistent with recently reported SFG experiments reported by Somorjai.[7−9,22] They indicate that even though the surface is significantly covered by the di-σ-intermediate, the π-bound species may in fact be the more favored reaction state at higher coverage conditions.

Conclusions

First-principle density functional theoretical calculations were used to help provide a more detailed atomic view of the ethylene chemisorption and hydrogenation on well-defined model Pd(111) systems. DFT results along with experimental results indicate that both and di-σ-bound ethylene intermediates are likely present on Pd. The computed adsorption energy for the di-σ-adsorption state is −60 kJ/mol on the Pd_{19} cluster (and −62 kJ/mol on the Pd(111) slab) while that for the π-bound

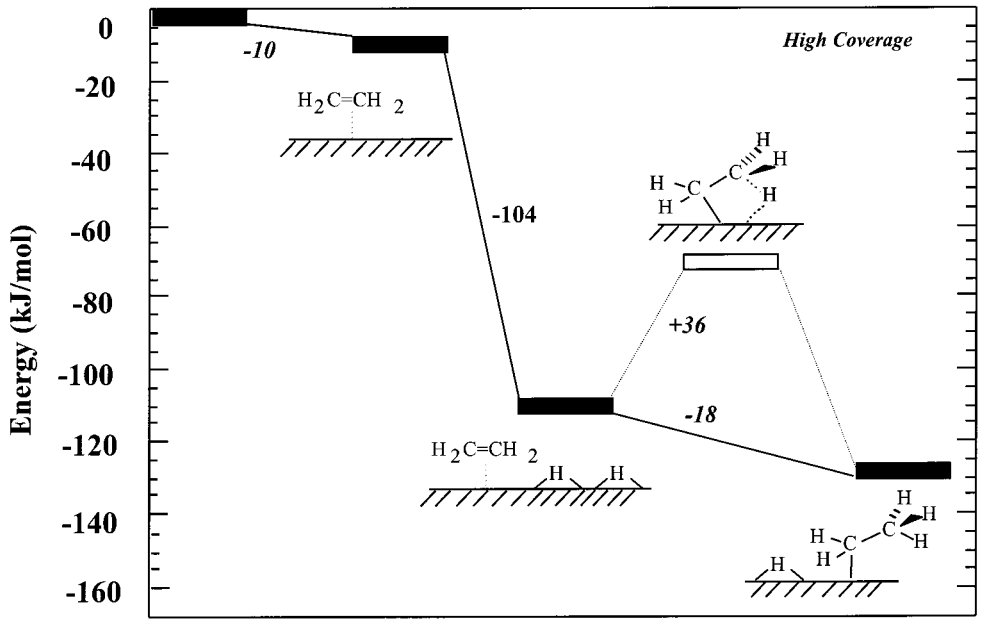

Figure 18. The overall potential energy diagram for ethylene hydrogenation over Pd(111) at high surface coverages. The solid boxes refer to reactant, intermediate and product states, whereas the two white boxes denote the transition state structures and energies for the surface reactions of ethylene to ethyl and ethyl to ethane.

state is −30 kJ/mol on Pd_{19} cluster (and −27 kJ/mol on the Pd(111) slab). Entropic considerations, however, become important as the temperature is increased. At higher temperatures, both the and di-σ-adsorption energies become quite similar. The π-bound state has a higher degree of rotational freedom than that for the di-σ-state. Hydrogenation of ethylene appears to follow the Horiuti−Polanyi mechanism of sequential hydrogen addition steps. At low surface coverages, the binding energy of ethyl, vinyl, and ethylidyne which are known intermediates involved in the selective hydrogenation paths and unselective decomposition routes are −130 (−140), −237 (−254), and −620 (−636) kJ/mol as computed from the DFT Pd_{19} cluster (and slab) calculations. At low coverage, ethylene was found to hydrogenate only from the di-σ-adsorption state. The isolated transition state is similar to that for other alkane activation steps proposed in the literature. The transition state for β-hydride C−H bond activation over the metal is late whereby there is a substantial stretch of the C−H bond before the metal surface will insert. The transition state for ethylene hydrogenation (reductive elimination) is identical due to microscopic reversibility. The calculated barrier was found to be +87 kJ/mol for the idealized state of infinite separation between ethylene and hydrogen in the reactant state. When the two surface species share a metal atom neighbor the barrier was reduced to +72 kJ/mol due to the repulsive interactions (+15 kJ/mol) between these species. At low coverage, the *apparent activation barriers* for the hydrogenation ethylene to ethyl, however, is only 27 kJ/mol, since it is measured with respect to the gas phase. The intrinsic reaction barrier for the subsequent hydrogenation of ethyl to ethane is +71 kJ/mol which is slightly lower in energy than that for the first hydrogenation step. The transition state is remarkably similar to that for ethylene hydrogenation. At lower coverages, the π-bound state was found to simply be a precursor intermediate to the di-σ-state.

At higher coverages, the nature of other surface intermediates such as oxygen, carbon, and ethylidyne all become more important as they can block adsorption sites and/or change the local electronic structure and hence surface reactivity. DFT results indicate that all of these intermediates are strongly bound to the surface. The calculated binding energies for O, C, and ethylidyne on the Pd_{19} cluster (and the Pd(111) slab) were −375 (−400), −610 (−635), −620 (−636) kJ/mol, respectively. Ethylidyne, which is strongly bound and readily present on the surface, behaves mainly as a spectator species in that it has a fairly low barrier for surface diffusion at +33 kJ/mol. Electronic interactions that occur through the metal and through-space strongly dictate the mode and energy of ethylene adsorption as well as its reactivity. If ethylene sits one metal surface bond away from other surface species, its binding energy is increased slightly due to through-surface attractive interactions. However, if ethylene shares metal atom sites with other surface intermediates, its interaction with the surface is reduced due to repulsive interactions. These repulsive interactions also act to lower the activation barrier. When ethylene and hydrogen are coadsorbed in $(\sqrt{3} \times \sqrt{3})$ $R30°$ coverages for both (0.6 ML), the activation barrier for the hydrogenation of ethylene to surface ethyl is reduced from +72 kJ/mol for the low coverage case to +36 kJ/mol for the higher coverage case. The computed barrier agrees quite well with known experimental values which range from 37 to 50 kJ/mol. The transition state for ethylene hydrogenation from the π-bound mode was only stable at higher coverages, and involved a "slip" like mechanism. The isolated transition state was found to be characteristically different than that which has been identified on homogeneous metal complexes in that the neighboring metal atom surface sites help to stabilize the transition state. The activation barriers for the classical homogeneous π-bound intermediate and the di-σ-adsorption state were found to be 84 and 32 kJ/mol higher than that for the surface-stabilized π-bound state.

Acknowledgment. M.N. thanks Mr. Venkataraman Pallassana and Mr. Eric Hansen for stimulating discussions and input. We kindly acknowledge the financial support from the DuPont Chemical Company, donors of the Petroleum Research Fund of the American Chemical Society (Grant 31342G5) and the National Science Foundation (Grant CTS-9702762). We also thank the NCSA at the University of Illinois at Urbana-Champaign for partial support of the computer time.

Appendix

TABLE A1: Total Energy Calculations for Pd_x ($x = 2-19$) Clusters

		singlet	triplet	quintet
palladium clusters				
Pd2	linear	−58.84826 2	−58.8599 79	
Pd5	trigonal bipyramidal	−145.754 6	−145.774 3	
	pyramid	−145.750 1	−145.772 9	
	planar	−145.707 9		
Pd6	octahedral	−174.937 11	−174.950 6	
	boat	−174.919 97	−174.945 8	
	prism	−174.918 8	−174.938 8	
	capped pentagon	−174.871 6	−174.917 2	
	planar	−174.871 6	−174.871 3	
Pd18		−554.065 071	−525.076 583	
Pd19		−554.2301	−554.266 735	−554.279 872
Pd23				−670.857 121
oxygen adsorption				
Pd−O		−104.246 11	−104.278 21	
Pd2−O		−133.459 50	−133.464 30	
Pd3−O		−162.625 02	−162.648 86	
Pd5−O		−220.835 72	−220.966 13	
Pd6−O		−220.969 43	−220.988 03	−220.962 803
Pd19_O_center		−629.43324	−629.444 714	
ethylene adsorption				
Pd19_C_2H_4_π-bound		−630.852 13	−632.875 820	

References and Notes

(1) (a) Ponec, V.; Bond, G. C. *Catalysis by Metals and Alloys*; Elsevier: Amsterdam, 1995; Vol. 95. (b) Marby, Prichard, M. W.; Ziemecki, S. U.S. Patent 4,550, 185 **1985**. (c) Landau, R. N.; Singh, U.; Gortsema, F.; Sun, Y.; Gomolka, S.; Larn, T.; Futran, M.; Blackmond, D. *J. Catal.* **1995**, *157*, 201−208.

(2) Mohsin, S. B.; Trenary, M.; Robota, H. J. *J. Phys. Chem.* **1988**, *92*, 5229−5233.

(3) Horiuti, J.; Polanyi, M. *Trans. Faraday Soc* **1934**, *30*, 1164.

(4) Farkas, A.; Farkas, L. *J. Am. Chem. Soc.* **1938**, *60*, 22.

(5) Zaera, F.; Somorjai, G. A. *J. Am. Chem. Soc.* **1984**, *106*, 2288.

(6) Beebe, T. P.; Yates, J. T. *J. Phys. Chem.* **1987**, *91*, 54−257.

(7) Cremer, P. S.; Somorjai, G. A. *J. Chem. Soc., Faraday Trans.* **1993**, *91*, 3671−3677.

(8) Cremer, P. S.; su, X.; Shen, Y. R.; Somorjai, G. A. *J. Am. Chem. Soc.* **1996**, *118*, 2942−2949.

(9) Cremer, P. S.; Su, X.; Ron Shen, Y.; Somorjai, G. A. *Catal. Lett* **1996**, *40*, 143−145.

(10) Yagasaki, E.; Masel, R. I. Variation in the Mechanism of Catalytic Reactions with Crystal Face. In *Catalysis*; Spivey, J. L., S. K. A., Ed.; Royal Society of Chemistry: Cambridge, 1994; Vol. 11, p 163.

(11) Bent, B. *Chem. Rev.* **1996**, *96*, 1361−1390.

(12) Zaera, F. *Chem. Rev.* **1995**, *95*, 2651−2693.

(13) Masel, R. I. *Principles of Adsorption and Reaction on Solid Surfaces*; J. Wiley Sons: New York, 1996.

(14) Tourillon, G.; Cassuto, A.; Jugnet, Y.; Massardier, J.; Bertolini, J. C. *J. Chem. Soc., Faraday Trans.* **1996**, *92*, 23, 4835−4841.

(15) Bertolini, J. C.; Cassuto, A.; Jugnet, Y.; Massardier, J.; Tardy, B.; Tourillon, G. *Surf. Sci.* **1996**, *349*, 88−96.

(16) Gates, J. A.; Kesmodel, L. L. *Surf. Sci.* **1982**, *120*, L461−L467.

(17) Gates, J. A.; Kesmodel, L. L. *Surf. Sci.* **1983**, *124*, 68−86.

(18) Tysoe, W. T.; Nyberg, G. L.; Lambert, R. M. *J. Phys. Chem.* **1984**, *88*, 1960−1963.

(19) Stuve, E. M.; Madix, R. J. *J. Phys. Chem.* **1985**, *89*, 105−112.

(20) Stuve, E. M.; Madix, R. J. *Surf. Sci.* **1985**, *160*, 293−304.

(21) Zaera, F.; N. Bernstein. *J. Am. Chem. Soc.* **1994**, *116*, 4881−4887.

(22) Cremer, P. S.; Somorjai, G. A. *J. Chem. Soc., Faraday. Trans.* **1995**, *91*, 3671−3677.

(23) Anderson, A. B.; Choe, S. J. *J. Phys. Chem.* **1989**, *93*, 6145−6149.

(24) Zaera, F. *Langmuir* **1996**, *12*, 88−94.

(25) Zaera, F.; Janssens, T. V. W.; Ofner, H. *Surf. Sci.* **1996**, *368*, 371−376.

(26) Merrill, P. B.; Madix, R. J. *J. Am. Chem. Soc.* **1996**, *118*, 5062−5067.

(27) Hansen, E. W.; Neurock, M. *Chem. Eng. Sci.* **1999**.

(28) Janssens, T. V. W.; Stone, D.; Hemminger, J. C.; Zaera, F. *J. Catal.* **1998**, *177*, 284−295.

(29) Kubota, J.; Ichihara, S.; Kondo, J. N.; Domen, K.; Hirose, C. *Langmuir* **1996**, *12*, 1926.

(30) Cassuto, A.; Kiss, J.; White, J. M. *Surf. Sci.* **1991**, *255*, 289.

(31) Zaera, F. *Langmuir* **1996**, *12*, 88.

(32) Reference deleted upon revision.

(33) Reference deleted upon revision.

(34) Reference deleted upon revision.

(35) Zaera, F.; Janssens, T. V. W.; Ofner, H. *Surf. Sci.* **1996**, *368*, 371.

(36) Yata, M.; Madix, R. J. *Surf. Sci.* **1995**, *328*, 171.

(37) Cremer, P.; Stanners, C.; Niemantserdriet, J. W.; Shen, Y. R.; Somorjai, G. A. *Surf. Sci.* **1995**, *328*, 111.

(38) Land, T. A.; Michely, T.; Behm, R.; Hemminger, J. C.; Comsa, G. *J. Chem. Phys.* **1992**, *97*, 6774.

(39) Hoffmann, R.; Silvestre, J. *Langmuir* **1985**, *1*, 621.

(40) Thorn, D. L.; Hoffmann, R. J. *J. Am. Chem. Soc.* **1978**, *97*, 4445.

(41) Sautet, P.; Paul, J. *Catal. Lett.* **1991**, *9*, 245−260.

(42) Blomberg, M. R. A.; Siegbahn, P. E. M.; Svensson, M. *J. Phys. Chem.* **1992**, *96*, 5783.

(43) Siegbahn, M. R. A. B.; Svensson, M. *J. Am. Chem. Soc.* **1993**, *115*, 1952.

(44) Siegbahn, P. E. M. *J. Am. Chem. Soc.* **1993**, *115*, 5803−5812.

(45) Paul, J. F.; Sautet, P. *Stud. Surf. Sci. Catal*. **1996**, *101*, 1253−1261.

(46) Neurock, M. *Stud. Surf. Sci. Catal*. **1997**, *109*, 3−31.

(47) Ge, Q.; King, D. A. *J. Chem. Phys.* **1999**, *110*, 4699−4702.

(48) Fahmi, A.; van Santen, R. A. *J. Phys. Chem.* **1996**, *100*, 5676−5680.

(49) Fahmi, A.; van Santen, R. A. *Surf. Sci.* **1997**, *371*, 53−62.

(50) Papai, I.; Ushio, J.; Salahub, D. R. *Surf. Sci.* **1993**, *282*, 262−272.

(51) Salahub, D. R.; Castro, M.; Proynov, E. I. Density Functional Theory, Its Gaussian Implementation and Applications to Complex Systems. In *NATO ASI, B318, Relativistic and Electron Correlation Effects in Molecules and Solid*; Malli, G. L., Ed.; Plenum Press: New York, 1994.

(52) van Santen, R. A.; Neurock, M. *Catal. Rev.* **1995**, *37*, 557.

(53) Andzelm, J.; Wimmer, E. *J. Chem. Phys.* **1992**, *96*, 1280−1303.

(54) Parr, R. G.; Yang, W. *Density Functional Theory of Atoms and Molecules*; Oxford University Press: Oxford, 1989.

(55) Salahub, D. R.; Fournier, R.; Mlynarski, P.; Papai, I.; St-Amant, A.; Ushio, J. *Gaussian-Based Density Functional Methodology, Software, and Applications*; Labinowski, J.A., Ed.; 1991.

(56) Vosko, S. H.; Wilk, L.; Nusair, M. *Can. J. Phys.* **1980**, *58*, 1200.

(57) Becke, A. D. *Phys. Rev. A* **1988**, *38*, 3098.

(58) Becke, A. *ACS Symp. Series* **1989**, *394*, 165.

(59) Perdew, J. P. *Phys. Rev. B* **1986**, *33*, 8822.

(60) Troullier, N.; Martins, J. L. *Phys. Rev. B* **1993**, 43.

(61) Andzelm, J.; Radzio, E.; Salahub+, D. R. *J. Comput. Chem.* **1985**, *6*, 520−532.

(62) Godbout, N.; Salahub, D. R.; Andzelm, J.; Wimmer, E. *Can. J. Chem.* **1992**, *70*, 560.

(63) Chen, H.; Krasowski, M.; Fitzgerald, G. **1993**, *98*, 8710.

(64) Nakao, T.; Dixon, D. A.; Chen, H. *J. Phys. Chem.* **1993**, *97*, 12665.

(65) Neurock, M.; Provine, W. D.; Dixon, D. A.; Coulston, G. W.; Lerou, J. J. *Chem. Eng. Sci.* **1996**, *51*, 1691−1699.

(66) Neurock, M.; Coulston, G. W.; Dixon, D. A. **1999**. In preparation.

(67) Neurock, M. *Top. Catal*. **1999**, *9*, 135−152.

(68) Neurock, M.; van Santen, R. A. Theory of Surface Chemical Reactivity. In *Handbook of Catalysis*; Ertl, G., Knozinger, H., Weitcamp, J., Ed.; Springer-Verlag, Inc.: 1996.
(69) Venkataraman, P.; Neurock, M.; Hansen, L. B.; Hammer, B.; Nørskov, J. K. *Phys. Rev. B* **1999**, *60*, 6146−6154.
(70) Hammer, B.; Hansen, L. B.; Nørskov, J. K. *Phys. Rev. B* **1999**.
(71) Chadi, D. J.; Cohen, M. L. *Phys. Rev. B* **1973**, *8*, 5747.
(72) Whitten, J. L.; Yang, H. *Surf. Sci. Rep.* **1996**, *218*, 55−124.
(73) Forbes, J. G.; Gellman, A. J. *J. Am. Chem. Soc.* **1993**, *115*, 6277.
(74) Jenks, C. J.; Bent, B. E.; Bernstein, N.; Zaera, F. *J. Am. Chem. Soc.* **1993**, *115*, 308.
(75) Zaera, F.; Tjandra, S.; Janssens, T. V. W. *Langmuir* **1998**, *14*, 1320.
(76) Zaera, F. *Acc. Chem. Res.* **1992**, *25*, 260−265.
(77) Solymosi, F.; Kovacs, I. *Surf. Sci.* **1991**, *259*, 95−108.
(78) Burghgraef, H.; Jansen, A. P. J.; van Santen, R. A. *J. Chem. Phys.* **1994**, *101*, 11012.
(79) Burghgraef, H.; Jansen, A. P. J.; van Santen, R. A. *Surf. Sci.* **1995**.
(80) Yang, H.; Whitten, J. L. *J. Am. Chem. Soc.* **1991**, *113*, 6442.
(81) Schule, J.; Siegbahn, P. E. M.; Wahlgren, U. *J. Chem. Phys.* **1988**, *89*, 6982.
(82) Siegbahn, P. E. M.; Panas, I. *Surf. Sci.* **1990**, *240*, 37.
(83) Kratzer, P.; Hammer, B.; Nørskov, J. K. *J. Chem. Phys.* **1996**, *105*, 5595−5604.
(84) Neurock, M.; van Santen, R. A. *J. Am. Chem. Soc.* **1994**, *116*, 4427−4439.
(85) Somorjai, G. A. *Introduction to Surface Chemistry and Catalysis*; J. Wiley: New York, 1994.
(86) Beebe, T. P.; Yates, J. T. *Surf. Sci. Lett.* **1986**, *173*, L606−L612.
(87) Wang, L. P.; Tysoe, W. T.; Ormerod, R. M.; Lambert, R. M.; Hoffmann, H.; Zaera, F. *J. Phys. Chem.* **1990**, *94*, 4236−4239.
(88) Kesmodel, L. L.; Gates, J. A. *Surf. Sci.* **1981**, *111*, L747−L754.
(89) Tysoe, W. T.; Nyberg, G. L.; Lambert, R. M. *J. Phys. Chem.* **1984**, *88*, 1960−1963.
(90) Natal-Santiago, M. A.; Podkolzin, S. G.; Cortright, R. D.; Dumesic, J. A. *Catal. Lett.* **1997**, *45*, 155−163.
(91) Passos, F. B.; Schmal, M.; Vannice, M. A. *J. Catal.* **1996**, *160*, 118−124.
(92) Freund, H. J. *Handbook of Heterogeneous Catalysis*; Ertl, G., Knozinger, H., Weitkamp, J., Eds.; Wiley-VCH: Weinheim, Germany, 1997; p 915.